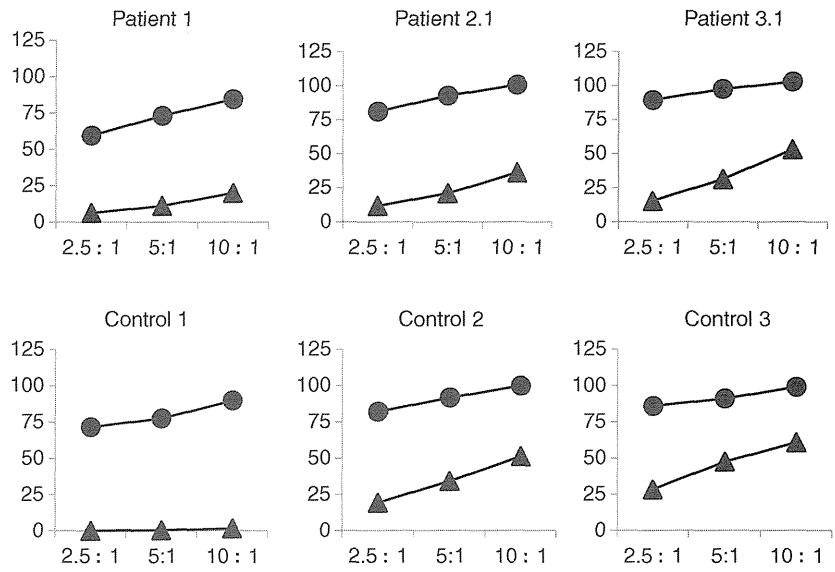

Fig. 5 Cytotoxicity of alloantigen-specific $CD8^+$ T cell lines. $CD8^+$ T cell lines were generated from PBMC of patients with XIAP deficiency and healthy controls by stimulation with allogeneic LCL (KI-LCL). Their cytotoxity was determined against allogeneic KI-LCL (*circles*) and against allogeneic TA-LCL (*triangles*), which does not share alloantigens with KI-LCL

XIAP deficiency was identified to be *XIAP/BIRC4*, and 25 mutations in the *XIAP* gene have been previously reported [7,12–14]. In the present study, we described four novel mutations (W217CfsX27, E349del, deletion of exons 1 and 2 and N341YfsX7) in the *XIAP* genes as well as previously described patients with R381X and R238X mutations [13,14]. The mother of patients 6.1 and 6.2 had no mutation in the *XIAP* gene. Because this is an X-linked inheritance, the failure to identify the same mutation in the mother suggests that the mother had a germline mosaicism for the mutation. Such mosaicism has not yet been described in XIAP deficiency, but it has been reported in Duchenne muscular dystrophy, X-linked severe combined immunodeficiency, X-linked agammaglobulinemia, and many other inherited diseases [24–26]. HLH is common in XIAP-deficient patients, and it is often recurrent [13,14]. In our study, six patients had HLH and five patients presented with recurrent HLH. Therefore, XIAP deficiency should be suspected in certain boys with HLH, especially in those with family history or recurrent HLH. The reason why XIAP deficiency increases susceptibility to HLH remains unclear. Murine studies have also failed to disclose a mechanism for the development of HLH [27]. Interestingly, Xiap-deficient mice possess normal lymphocyte apoptosis induced by a variety of means [28]. Three of our patients presented with EBV-associated HLH. EBV infection has been reported to be a trigger of the first HLH episode in patients with XIAP deficiency [13]. The excess of lymphocyte apoptosis in XIAP deficiency might account for the abnormal immune response to EBV [28]. Splenomegaly is not frequently observed in XLP type 1 or SAP deficiency but might be a common clinical feature in XIAP deficiency [12,13] as four (50%) of eight Japanese patients developed splenomegaly. Pachlopnik Schmid et al. [13] reported that recurrent splenomegaly occurring in the absence of systemic HLH was often associated with fever and cytopenia. XIAP-deficient patients are at risk for chronic colitis, which is possibly a more frequent cause of mortality than HLH [13]. Our study included two patients who developed colitis, and one of the patients died of colitis at 4 years of age. Although we did not have enough clinical information or samples from that patient because of his early death, his symptoms suggest that he had a XIAP deficiency complicated with colitis because he was the maternal uncle of patient 2.1. The other patient was 2 years old and also suffered from chronic hemorrhagic colitis.

In contrast to SAP deficiency, lymphoma has never been reported in XIAP deficiency, including our patients. Some studies indicate that the XIAP protein is a potential target for the treatment of cancer based on the anti-apoptotic function of XIAP [29]. Therefore, the absence of XIAP may protect patients from cancer, explaining why XIAP-deficient patients do not develop lymphoma. We generated a clinical summary to compare XIAP-deficient patients with the previous reports (Table II). Although our study included a relatively small number of patients, our results appear to be consistent with previous large studies [12,13] and confirm the clinical characteristics of XIAP deficiency.

Flow cytometry can be used for the rapid screening of several primary immunodeficiencies including XLP [30]. XIAP protein has been found to be expressed in various human tissues, including all hematopoietic cells [7,10]. Marsh et al. [16] described that XIAP was readily detectable in normal granulocytes, monocytes, and all lymphocyte subsets. Moreover, patients with *XIAP* mutations had decreased or absent expression of XIAP protein by flow cytometry [14,16]. We investigated XIAP expression in lymphocytes from eight patients by flow cytometry as previously described [16,17]. As demonstrated by Marsh et al. [16], clone 48 antibody provided brighter staining compared

Table II Comparison of patients with XIAP deficiency

	Marsh R et al. [12]	Pachlopnik Schmid J et al. [13]	Our study
Number of patients	10	30	9
HLH	9 (90%)	22/29 (76%)	6/9 (67%)
Recurrent HLH	6 (60%)	11/18 (61%))	5/6 (83%)
EBV-associated HLH	3 (30%)	16/19 (84%)	4/6 (67%)
Splenomegaly	9 (90%)	19/21 (90%)	4/8 (50%)
Hypogammaglobulinema	2 (20%)	8/24 (33%)	2/8 (25%)
Lymphoma	0	0	0
Colitis	0	5 (17%)	2 (22%)

to clone 2F1 antibody. In patients 5, 6.1, and 6.2, XIAP protein expression was normal when using clone 48 antibody but decreased when using clone 2F1 antibody. Western blot analysis showed XIAP expression in patients 3.1, ,5 and 6.2, and using clone 48 antibody, we found a discrepancy between flow cytometry and Western blot. Flow cytometric diagnosis may thus result in false positive results, and the gene sequencing of *XIAP* should be performed even when the patient shows normal XIAP expression levels.

All of the mothers examined in this study except for one were carriers of *XIAP* mutations. Analysis of XIAP expression in the mothers of patients 1, 3.1, and 3.2 revealed a bimodal expression pattern of XIAP in lymphocytes with cellular skewing towards expression of the wild-type XIAP allele as previously demonstrated [16]. However, the mother of patients 2.1, 6.1, and 6.2 demonstrated a normal expression pattern, possibly resulting from an extremely skewed pattern of X chromosome inactivation as shown in XIAP deficiency and other primary immunodeficiencies, and de novo mutations in *XIAP* are also observed [16,31]. The mother of patients 6.1 and 6.2 might have a germline mosaicism for the mutation, resulting in normal XIAP protein expression.

iNKT cells represent a specialized T lymphocyte subpopulation with unique features distinct from conventional T cells [32,33]. Human iNKT cells express an invariant TCR that recognizes self and microbacterial glycosphingolipid antigens presented by the major histocompatibility complex class I-like molecule CD1d [28]. The first series of XIAP-deficient patients showed decreased iNKT cell counts similar to SAP deficiency [7]. However, Xiap-deficient mice have normal numbers of iNKT cells and did not show an abnormal response to apoptotic stimuli [34]. Marsh et al. [23] reported a cohort of XIAP-deficient patients with normal numbers of iNKT cells, indicating that XIAP-deficient patients differ from SAP-deficient patients in this respect. In our cohort, we observed significantly decreased iNKT cell numbers in XIAP-deficient patients compared to healthy controls. However, we could not identify a correlation between the number of iNKT cells and the clinical disease features. Flow cytometric evaluation of iNKT cell counts can allow for the discrimination of XLP and other primary immunodeficiency diseases because patients may have normal XIAP protein expression in their lymphocytes.

CTLs kill their targets by one of two mechanisms: granule- or receptor-mediated apoptosis [35]. A recent study showed that the main pathway of cytotoxicity mediated by alloantigen-specific human $CD4^+$ and $CD8^+$ T cells is granule exocytosis and not the FAS/FAS ligand system [18]. Granzyme B is a major effector molecule of granule-mediated killing that rapidly induces cell death after entering the cytoplasm of the target cell [36]. The enzymatic activity of granzyme B is key to its ability to induce cell death. The executioner caspase-3 has been shown to be proteolytically processed and activated by granzyme B [37]. Although XIAP possesses an inhibitory effect for caspases, it is important to study the cytotoxic activities of CTLs in XIAP deficiency. Furthermore, many studies have indicated that some subtypes of patients with familial HLH show a deficiency in their cytotoxic activities [20,38]. To further investigate the function of antigen-specific CTLs, we studied $CD8^+$ alloantigen-specific CTL analysis among three XIAP-deficient patients. XIAP-deficient patients showed a normal level of cytotoxic activity, suggesting that XIAP might not play an important role in the cytotoxic responses of $CD8^+$ T cells as was previously suggested based on the normal NK cell-mediated cytotoxicity found in XIAP-deficient patients [7,12].

In this study, we have described nine Japanese patients with XIAP deficiency with clinical characteristics similar to those of patients in Europe and USA [12,13].

Acknowledgments This study was supported by Grant-in-Aids for Scientific Research from the Ministry of Education, Culture, Sports, Science and Technology (H. Kanegane and T. Miyawaki) and grants from the Ministry of Health, Labour, Welfare of Japan (T. Miyawaki), the XLP Reserch Trust (S. Latour) and Agence Nationale pour la Recherche (ANR-08-MIEN-012-01) and an Erasmus MC Fellowship (M.C. van Zelm). We thank Ms. Chikako Sakai and Mr. Hitoshi Moriuchi for their excellent technical assistance. We are also grateful for the support, cooperation, and trust of the patients and their families.

References

1. Sumegi J, Huang D, Lanyi A, Davis JD, Seemayer TA, Maeda A, et al. Correlation of mutations of the SH2D1A gene and Epstein–Barr virus infection with clinical phenotype and outcome in X-linked lymphoproliferative disease. Blood. 2000;96:3118–25.
2. Seemayer TA, Gross TG, Egeler RM, Pirruccello SJ, Davis JR, Kelly CM, et al. X-linked lymphoproliferative disease: twenty-five years after the discovery. Pediatr Res. 1995;38:471–8.
3. Sayos J, Wu C, Morra M, Wang N, Zhang X, Allen D, et al. The X-linked lymphoproliferative-disease gene product SAP regulates signals induced through the co-receptor SLAM. Nature. 1998;395:462–9.
4. Coffey AJ, Brooksbank RA, Brandau O, Oohashi T, Howell GR, Bye JM, et al. Host response to EBV infection in X-linked lymphoproliferative disease results from mutations in an SH2-domain encoding gene. Nat Genet. 1998;20:129–35.
5. Nichols KE, Harkin DP, Levitz S, Krainer M, Kolquist KA, Genovese C, et al. Inactivating mutations in an SH2 domain-encoding gene in X-linked lymphoproliferative syndrome. Proc Natl Acad Sci USA. 1998;95:13765–70.
6. Gilmour KC, Cranston T, Jones A, Davies EG, Goldblatt D, Thrasher A, et al. Diagnosis of X-linked lymphoproliferative disease by analysis of SLAM-associated protein expression. Eur J Immunol. 2000;30:1691–7.
7. Rigaud S, Fondanèche MC, Lambert N, Pasquier B, Mateo V, Soulas P, et al. XIAP deficiency in humans causes an X-linked lymphoproliferative syndrome. Nature. 2006;444:110–4.
8. Uren AG, Pakusch M, Hawkins CJ, Puls KL, Vaux DL. Cloning and expression of apoptosis inhibitory protein homologs that function to inhibit apoptosis and/or bind tumor necrosis factor receptor-associated factors. Proc Natl Acad Sci USA. 1996;93:4974–8.
9. Liston P, Roy N, Tamai K, Lefebvre C, Baird S, Cherton-Horvat G, et al. Suppression of apoptosis in mammalian cells by NAIP and a related family of IAP genes. Nature. 1996;379:349–53.
10. Duckett CS, Nava VE, Gedrich RW, Clem RJ, van Dongen JL, Gilfillan MC, et al. A conserved family of cellular genes related to the baculovirus iap gene and encoding apoptosis inhibitors. EMBO J. 1996;15:2685–94.
11. Galbán S, Duckett CS. XIAP as a ubiquitin ligase in cellular signaling. Cell Death Differ. 2010;17:54–60.
12. Marsh RA, Madden L, Kitchen BJ, Mody R, McClimon B, Jordan MB, et al. XIAP deficiency: a unique primary immunodeficiency best classified as X-linked familial hemophagocytic lymphohistiocytosis and not as X-linked lymphoproliferative disease. Blood. 2010;7:1079–82.
13. Pachlopnik Schmid J, Canioni D, Moshous D, Touzot F, Mahlaoui N, Hauck F, et al. Clinical similarities and differences of patients with X-linked lymphoproliferative syndrome type 1 (XLP-1/SAP-deficiency) versus type 2 (XLP-2/XIAP-deficiency). Blood. 2011;117:1522–9.
14. Zhao M, Kanegane H, Ouchi K, Imamura T, Latour S, Miyawaki T. A novel XIAP mutation in a Japanese boy with recurrent pancytopenia and splenomegaly. Haematologica. 2010;95:688–9.
15. Filipovich AH, Zhang K, Snow AL, Marsh RA. X-linked lymphoproliferative syndromes: brothers or distant cousins? Blood. 2010;116:3398–408.
16. Marsh RA, Villanueva J, Zhang K, Snow AL, Su HC, Madden L, et al. A rapid flow cytometric screening test for X-linked lymphoproliferative disease due to XIAP deficiency. Cytometry B Clin Cytom. 2009;76:334–44.
17. Marsh RA, Bleesing JJ, Filipovich AH. Using flow cytometry to screen patients for X-linked lymphoproliferative disease due to SAP deficiency and XIAP deficiency. J Immunol Methods. 2010;362:1–9.
18. Yasukawa M, Ohminami H, Arai J, Kasahara Y, Ishida Y, Fujita S. Granule exocytosis, and not the fas/fas ligand system, is the main pathway of cytotoxity mediated by alloantigen-specific CD4(+) as well as CD8(+) cytotoxic T lymphocytes in humans. Blood. 2000;95:2352–5.
19. Yanai F, Ishii E, Kojima K, Hasegawa A, Azuma T, Hirose S, et al. Essential roles of perforin in antigen-specific cytotoxity mediated by human CD4+ T lymphocytes: analysis using the combination of hereditary perforin-deficient effector cells and Fas-deficient target cells. J Immunol. 2003;170:2205–13.
20. Ishii E, Ueda I, Shirakawa R, Yamamoto K, Horiuchi H, Ohga S, et al. Genetic subtypes of familial hemophagocytic lymphohistiocytosis: correlations with clinical features and cytotoxic T lymphocyte/natural killer cell functions. Blood. 2005;105:3442–8.
21. Nichols KE, Hom J, Gong SY, Ganguly A, Ma CS, Cannons JL, et al. Regulation of NKT cell development by SAP, the protein defective in XLP. Nat Med. 2005;11:340–5.
22. Pasquier B, Yin L, Fondanéche MC, Relouzat F, Bloch-Queyrat C, Lambert N, et al. Defective NKT cell development in mice and humans lacking the adapter SAP, the X-linked lymphoproliferative syndrome gene product. J Exp Med. 2005;201:695–701.
23. Marsh RA, Villanueva J, Kim MO, Zhang K, Marmer D, Risma KA, et al. Patients with X-linked lymphoproliferative disease due to *BIRC4* mutation have normal invariant natural killer T-cell populations. Clin Immunol. 2009;132:116–23.
24. Puck JM, Pepper AE, Bedard PM, Laframboise R. Female germ line mosaicism as the origin of a unique IL-2 receptor gamma-chain mutation causing X-linked severe combined immunodeficienc. J Clin Invest. 1995;95:895–9.
25. O'Marcaigh A, Puck JM, Pepper AE, Santes KD, Cowan MJ. Maternal mosaicism for a novel interleukin-2 receptor gamma-chain mutation causing X-linked severe combined immunodeficiency in a Navajo kindred. J Clin Immunol. 1997;17:29–33.
26. Sakamoto M, Kanegane H, Fujii H, Tsukada S, Miyawaki T, Shinomiya N. Maternal germinal mosaicism of X-linked agammaglobulinemia. Am J Med Genet. 2001;99:234–7.
27. Harlin H, Reffey SB, Duckett CS, Lindsten T, Thompson CB. Characterization of XIAP-deficient mice. Mol Cell Biol. 2001;21:3604–8.
28. Latour S. Natural killer T cells and X-linked lymphoproliferative syndrome. Curr Opin Allergy Clin Immunol. 2007;7:510–4.
29. Schimmer AD, Dalili S, Batey RA, Riedl SJ. Targeting XIAP for the treatment of malignancy. Cell Death Differ. 2006;13:179–88.
30. Oliveira JB, Notarangelo LD, Fleisher TA. Applications of flow cytometry for the study of primary immune deficiencies. Curr Opin Allergy Clin Immunol. 2008;8:499–509.
31. Kanegane H, Futatani T, Wang Y, Nomura K, Shinozaki K, Matsukura H, et al. Clinical and mutational characteristics of X-linked agammaglobulinemia and its carrier identified by flow cytometric assessment combined with genetic analysis. J Allergy Clin Immunol. 2001;108:1012–20.
32. Godfrey DI, Berzins SP. Control points in NKT-cell development. Nat Rev Immunol. 2007;7:505–18.
33. Bendelac A, Savage PB, Teyton L. The biology of NKT cells. Annu Rev Immunol. 2007;25:297–336.
34. Bauler LD, Duckett CS, O'Riordan MX. XIAP regulates cytosol-specific immunity to *Listeria* infection. PLoS Pathog. 2008;4:e1000142.
35. Hersperger AR, Makedonas G, Betts MR. Flow cytometric detection of perforin upregulation in human CD8 T cells. Cytometry A. 2008;73:1050–7.
36. Motyka B, Korbutt G, Pinkoski MJ, Heibein JA, Caputo A, Hobman M, et al. Mannose 6-phosphate/insulin-like growth

factor II receptor is a death receptor for granzyme B during cytotoxic T cell-induced apoptosis. Cell. 2000;103:491–500.
37. Martin SJ, Amarante-Mendes GP, Shi L, Chuang TH, Casiano CA, O'Brien GA, et al. The cytotoxic cell protease granzyme B initiates apoptosis in a cell-free system by proteolytic processing and activation of the ICE/CED-3 family protease, CPP32, via a novel two-step mechanism. EMBO J. 1996;15:2407–16.
38. zur Stadt U, Rohr J, Seifert W, Koch F, Grieve S, Pagel J, et al. Familial hemophagocytic lymphohistiocytosis type 5 (FHL-5) is caused by mutations in Munc18-2 and impaired binding to syntaxin 11. Am J Hum Genet. 2009;85:482–92.

Chronic Mucocutaneous Candidiasis Caused by a Gain-of-Function Mutation in the STAT1 DNA-Binding Domain

Shunichiro Takezaki,*[,1] Masafumi Yamada,*[,1] Masahiko Kato,[†] Myoung-ja Park,[‡] Kenichi Maruyama,[§] Yasuhiro Yamazaki,* Natsuko Chida,*[,¶] Osamu Ohara,[‖] Ichiro Kobayashi,* and Tadashi Ariga*

Chronic mucocutaneous candidiasis (CMC) is a heterogeneous group of primary immunodeficiency diseases characterized by chronic and recurrent *Candida* infections of the skin, nails, and oropharynx. Gain-of-function mutations in *STAT1* were very recently shown to be responsible for autosomal-dominant or sporadic cases of CMC. The reported mutations have been exclusively localized in the coiled-coil domain, resulting in impaired dephosphorylation of STAT1. However, recent crystallographic analysis and direct mutagenesis experiments indicate that mutations affecting the DNA-binding domain of STAT1 could also lead to persistent phosphorylation of STAT1. To our knowledge, this study shows for the first time that a DNA-binding domain mutation of c.1153C>T in exon 14 (p.T385M) is the genetic cause of sporadic CMC in two unrelated Japanese patients. The underlying mechanisms involve a gain of STAT1 function due to impaired dephosphorylation as observed in the coiled-coil domain mutations. *The Journal of Immunology*, 2012, 189: 1521–1526.

Chronic mucocutaneous candidiasis (CMC) is a heterogeneous group of primary immunodeficiency diseases characterized by chronic and recurrent *Candida* infections of the skin, nails, and oropharynx (1). It is often associated with a variety of endocrine or autoimmune disorders. Especially, in autoimmune polyendocrinopathy with candidiasis and ectodermal dystrophy, mucocutaneous candidiasis is accompanied by hypoparathyroidism, adrenal failure, insulin-dependent diabetes mellitus, alopecia, and malabsorption syndrome (2). Although autosomal-dominant forms of CMC are also associated with endocrine disorders, such as hypothyroidism (3), the genetic causes of these disorders had remained unknown until very recently.

In 2011, two groups reported that autosomal-dominant CMC and sporadic CMC are caused by mutations in *STAT1* (4–6). The reported mutations have been exclusively localized in the coiled-coil (CC) domain, leading to gain of STAT1 function due to impaired STAT1 dephosphorylation (4). However, crystallographic analysis and direct mutagenesis experiments indicated that mutations in the DNA-binding domain (DBD) could also cause a resistance to dephosphorylation (7, 8). To our knowledge, this is the first study to demonstrate that a mutation affecting the DBD of STAT1 is the genetic cause of sporadic CMC in two unrelated Japanese patients. The mechanisms involve a gain of STAT1 function due to impaired dephosphorylation of STAT1, as also observed in mutations affecting the CC domain.

Materials and Methods

Patients

Patient 1 is a 12-y-old boy born to nonconsanguineous healthy Japanese parents. He developed severe and recurrent oral thrush since the age of 2 y and was diagnosed with CMC. He has also had recurrent pneumonia, bronchitis, and otitis media caused by *Streptococcus pneumoniae* since the age of 3 y. Chest x-ray and computerized tomography scan demonstrated the presence of bronchiectasis at the age of 5 y. He was noticed to have hypothyroidism with positive anti–thyroid-stimulating hormone receptor Abs, and levothyroxine was initiated at the age of 9 y.

Patient 2 is a boy born to nonconsanguineous healthy Japanese parents. He had poor body weight gain soon after birth. He was diagnosed with CMC at the age of 6 y. He also had recurrent bronchitis, pneumonia, and sinusitis caused by *S. pneumoniae*. He was diagnosed with bronchiectasis at the age of 7 y. At the age of 13 y, he developed hemophagocytic lymphohistiocytosis (HLH). He subsequently presented with autoimmune hemolytic anemia with positive direct and indirect Coombs' tests and thrombocytopenia and was diagnosed as having Evans syndrome. He died suddenly at the age of 14 y and 5 mo from disseminated intravascular coagulation and pulmonary insufficiency of unknown etiology. These two patients were not related (case reports in preparation).

Patient 3 is a 15-y-old girl with CMC. Her father had also been diagnosed with CMC and died of cerebral vasculitis (9). She was demonstrated to have the heterozygous R274Q mutation affecting the CC domain of STAT1. Because this mutation was recently reported as a gain-of-function mutation due to impaired dephosphorylation of STAT1 (4), we studied Patient 3 as a control for investigating the mechanisms of the development of CMC in Patients 1 and 2. Informed consent for genetic analysis was obtained from the patients, their family members, and normal controls under a protocol approved by the Institutional Review Board of Hokkaido University Hospital.

*Department of Pediatrics, Hokkaido University Graduate School of Medicine, Sapporo 060-8638, Japan; [†]Department of Allergy and Immunology, Gunma Children's Medical Center, Shibukawa 377-8577, Japan; [‡]Department of Hematology/Oncology, Gunma Children's Medical Center, Shibukawa 377-8577, Japan; [§]Department of Nephrology, Gunma Children's Medical Center, 377-8577, Shibukawa, Japan; [¶]Department of Dentistry for Children and Disabled Persons, Hokkaido University Graduate School of Dental Medicine, Sapporo 060-8586, Japan; and [‖]Department of Human Genome Technology, Kazusa DNA Research Institute, Chiba 292-0818, Japan

[1]S.T. and M.Y. contributed equally to this work.

Received for publication March 28, 2012. Accepted for publication May 25, 2012.

This work was supported in part by a grant for Research on Intractable Diseases from the Japanese Ministry of Health, Labor and Welfare and a grant from the Hokkaido University Frontier Foundation.

Address correspondence and reprint requests to Dr. Masafumi Yamada, Department of Pediatrics, Hokkaido University Graduate School of Medicine, North 15 West 7, Kita-ku, Sapporo 060-8638, Japan. E-mail address: yamadam@med.hokudai.ac.jp

Abbreviations used in this article: CC, coiled-coil; CMC, chronic mucocutaneous candidiasis; DBD, DNA-binding domain; HLH, hemophagocytic lymphohistiocytosis; STAT1p, phosphorylated STAT1; Wt, wild-type.

www.jimmunol.org/cgi/doi/10.4049/jimmunol.1200926

Generation of EBV-transformed cell lines

EBV-transformed cell lines (EBV-LCLs) were generated by in vitro transformation of human B cells with EBV (strain B95-8), as described elsewhere (10). Based on the results of *STAT1* sequence analysis, EBV-LCLs from Patient 1 with T385M and wild-type (Wt) alleles and Patient 3 with R274Q and Wt alleles were designated as T385M/Wt and R274Q/Wt, respectively. Two age-matched control EBV-LCLs, designated Wt-1 and Wt-2, were used as controls. EBV-LCLs from Patient 2 were not obtained.

Stimulation reagents

For stimulation, 1:1000 diluted recombinant human IFN-γ 1a (Shionogi, Osaka, Japan; 1000 JRU/ml, 200 ng/ml), 1500 U/ml recombinant human IFN-α (Biosource International, Camarillo, CA), 20 ng/ml IL-27 (R&D Systems, Minneapolis, MN), and 100 μg/ml Curdlan (Wako, Osaka, Japan) were used.

DNA isolation, PCR, and sequence analysis of PCR products and TOPO-TA clones

These procedures were performed following the methods described elsewhere (10).

Measurement of CXCL10 (IP-10) concentration in supernatant of monocyte-derived macrophages and EBV-LCLs using Cytometric Bead Array

To accurately evaluate STAT1 function by studying supernatant IP-10 production from macrophages, monocytes were first purified from PBMCs with CD14 MicroBeads (Miltenyi Biotec, Bergisch Gladbach, Germany) to avoid contamination of other cells. A total of 5×10^5 cells/ml monocytes was then differentiated into macrophages by culturing for 7 d in RPMI 1640 containing 10% FBS in the presence of 5 ng/ml M-CSF (R&D Systems). To determine the effect of IFN-γ, differentiated macrophages in triplicate were not stimulated, were stimulated with 1 μg/ml LPS (Sigma, St Louis, MO), or were prestimulated with 1000 U/ml (200 ng/ml) IFN-γ (Shionogi) for 2 h and then stimulated with 1 μg/ml LPS for 24 h (IFN-γ–LPS stimulation), and supernatant was harvested for IP-10 measurement. For studying IP-10 production from EBV-LCLs, 1×10^6 cells/ml EBV-LCLs were cultured in the presence of 1000 U/ml IFN-γ for 6 h. The concentration of IP-10 in the supernatant was measured with Cytometric Bead Array (BD, San Diego, CA), following the manufacturer's instructions. Data from triplicate independent experiments are reported as the mean ± SD.

Preparation of nuclear extract

Nuclear extract was prepared essentially as described previously (11). Briefly, harvested cells were washed with Ca^{2+} and Mg^{2+}-free PBS and pelleted by centrifugation at 1500 × *g* for 5 min at 4°C. The resulting cell pellets were resuspended in cytoplasmic extract buffer (10 mM HEPES [pH 7.9], 10 mM KCl, 0.1 mM EDTA, 0.1 mM EGTA, 1 mM DTT, 1 mM Na_3VO_4, 1 mM NaF [pH 8]) with the addition of the recommended volume of dissolved protease inhibitor mixture tablets (Roche). After incubation on ice for 15 min, a 1:16 volume of 10% Nonidet P-40 was added. The suspension was vortexed and then centrifuged at 1500 × *g* for 5 min at 4°C. The pellets were washed again with cytoplasmic extract buffer without Nonidet P-40, resuspended with nuclear extract buffer (20 mM HEPES [pH 7.9], 400 mM NaCl, 1 mM EDTA, 1 mM EGTA, 1 mM DTT, 1 mM Na_3VO_4, 1 mM NaF [pH 8]) with the addition of protease inhibitor, and incubated at 4°C for 30 min. After centrifugation at maximum speed for 5 min at 4°C, the supernatant was saved as nuclear extract. Protein concentration was measured by Protein Assay (Bio-Rad, Hercules, CA).

Western blot analysis

After addition of SDS sample buffer, 10 μg nuclear extract was separated by 7.5% polyacrylamide gels and transferred to Immobilon-P Transfer Membranes (Millipore, Billerica, MA). Anti-lamin A Ab (BioLegend, San Diego, CA) was used as a loading control for nuclear extract. All of the primary Abs were used at the final concentration of 1 μg/ml. HRP-conjugated anti-mouse IgG secondary Abs (GE Healthcare, Buckinghamshire, U.K.) were used at 1:2000 dilution. The blots were then visualized by Pierce Western blotting Substrate (Thermo, Rockford, IL).

Studies of STAT1 phosphorylation state and staurosporine and pervanadate treatment of cells

We assessed dephosphorylation with the tyrosine kinase inhibitor staurosporine in EBV-LCLs. A total of 1×10^6 cells/ml EBV-LCLs was stimulated with IFN-γ for 30 min and then incubated with 1 μM staurosporine (Alomone Labs, Jerusalem, Israel) for 15, 30, or 60 min. The phosphatase inhibitor pervanadate was prepared by mixing 200 mM sodium orthovanadate (Wako, Osaka, Japan) and 100 mM H_2O_2 at a 2:1 ratio for 15 min at 22°C. EBV-LCLs were treated with pervanadate (0.8 mM orthovanadate and 0.2 mM H_2O_2) for 5 min and then stimulated with IFN-γ for 30 min. The nuclear extract from each condition was subjected to SDS-PAGE. The phosphorylation state of STAT1 was evaluated with anti-human STAT1 (pY701) Ab purchased from BD. The membrane was then stripped and reprobed with anti-human STAT1 (BD) and anti-lamin A (BioLegend) Abs.

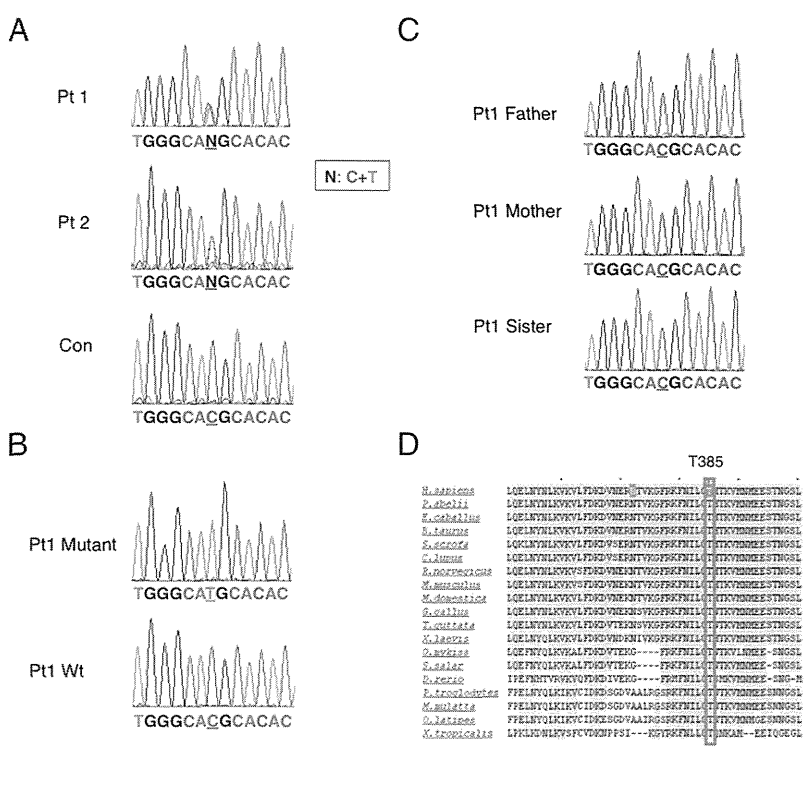

FIGURE 1. Patients 1 and 2 had the same heterozygous base change of c.1153C>T resulting in p.T385M in *STAT1*. (**A**) Direct sequence analysis of *STAT1* exon 14 in Patient 1 (Pt1) and Patient 2 (Pt2). Forward sequence is shown. (**B**) Sequence analysis of TOPO-TA clones of *STAT1* exon 14 PCR products in Patient 1. Mutant and Wt sequences are shown. (**C**) Direct sequence analysis of *STAT1* exon 14 in Patient 1's family members. (**D**) Comparison of the amino acid sequences of STAT1 in different species. The red box indicates the amino acids corresponding to p.T385 in humans. Con, Control.

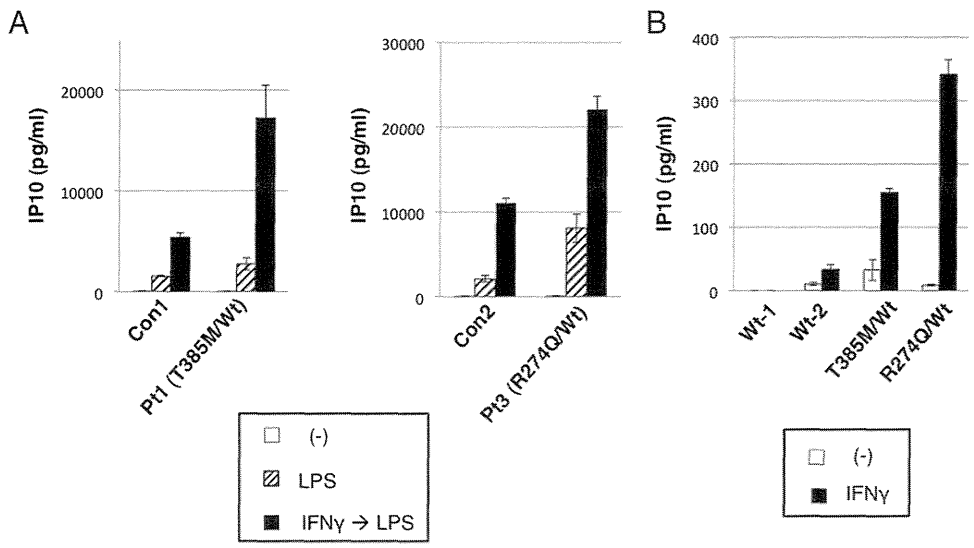

FIGURE 2. T385M was associated with higher levels of IP-10 production following IFN-γ stimulation in monocyte-derived macrophages and in EBV-LCLs. (**A**) Monocyte-derived macrophages were cultured in the presence of media, LPS, or IFN-γ–LPS for 24 h. IP-10 production was studied in the supernatant. Data shown are mean ± SD of triplicate independent experiments. (**B**) EBV-LCLs were stimulated with IFN-γ for 6 h, and IP-10 production was studied in the supernatant. Data shown are mean ± SD of triplicate independent experiments. Con1, Control for Patient 1 obtained and analyzed at the same time; Con2, control for Patient 3 obtained and analyzed at the same time; Pt1, Patient 1; Pt3, Patient 3; (−), media.

Flow cytometric analysis of intracellular IL-17A expression in CD4$^+$ cells

PBMCs at a density of 1 × 10^6 cells/ml were stimulated with 20 ng/ml PMA plus 500 ng/ml ionomycin for 6 h in the presence of GolgiStop (BD). Harvested PBMCs were washed and stained with PECy5-conjugated anti-human CD4 Ab (BioLegend) for 20 min at 4°C. Cells were washed three times and fixed and permeabilized with Cytofix/Cytoperm solution (BD) for 20 min at 4°C. Cells were then washed, incubated for 30 min with PE-conjugated anti-human IL-17A (BioLegend) or FITC-conjugated anti-human IFN-γ Abs (BioLegend), washed, and analyzed with a FACSCalibur (BD).

Results

A possible DBD mutation in STAT1

We first performed direct sequence analysis of the genes responsible for CMC in our patients: *AIRE*, *CLEC7A*, *CARD9*, *IL17RA*, *IL17F*, *IL2Rα*, and *STAT1* (4–6, 12–17). This study demonstrated that Patient 1 and Patient 2 have the same heterozygous base change in *STAT1* (c.1154C>T, p.T385M) (Fig. 1A), which was confirmed by the sequence analysis of TOPO-TA clones (Fig. 1B, data not shown). This base change has not been reported either as a mutation or as a single nucleotide polymorphism in the National Center for Biotechnology Information database, Ensembl database, or the Single Nucleotide Polymorphism Database, and it was not present in the family members of Patient 1 (Fig. 1C) or in 108 normal healthy controls (data not shown). Furthermore, the affected residue was evolutionarily conserved, as shown in Fig. 1D. The polymorphism phenotype-2 (PolyPhen-2) algorithm (http://genetics.bwh.harvard.edu/pph2/index.shtml), a structure sequence-based amino acid substitution-prediction method, predicted p.T385M as probably damaging, with a score of 1.000 (sensitivity: 0.00; specificity: 1.00). The sort intolerant from tolerant algorithm (http://sift.jcvi.org/) also predicted this amino acid substitution as deleterious. These results strongly indicate that c.1153C>T (p.T385M) is a de novo disease-causing mutation. Patient 1 was also shown to have an unreported heterozygous base change in *CARD9* (c.661G>A, p.K221E). However, this base change was also detected in his healthy father (data not shown). Additionally, PBMCs from Patient 1 showed normal IL-6 production in response

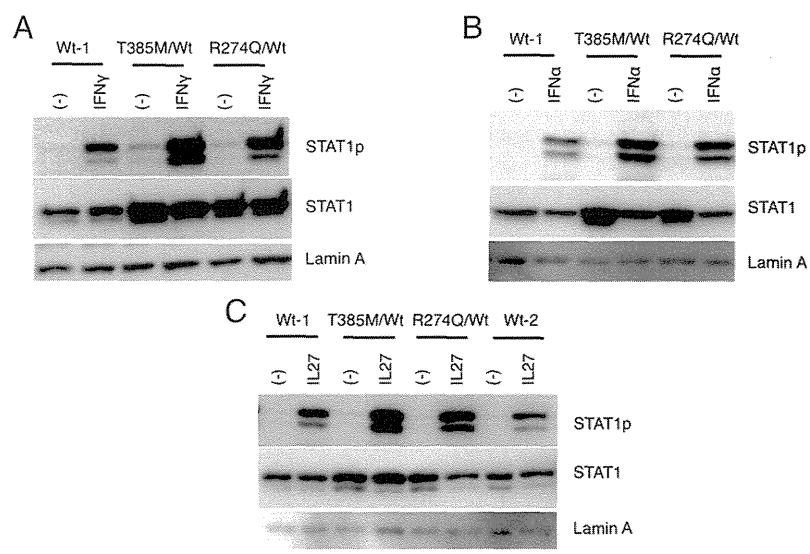

FIGURE 3. T385M was associated with hyperphosphorylation of STAT1 in response to IFN-γ, IFN-α, and IL-27 stimulation. Western blot analysis of STAT1p in nuclear extracts from EBV-LCLs was performed. Lamin A was used as a loading control. STAT1p expression in EBV-LCLs following IFN-γ (**A**), IFN-α (**B**), or IL-27 (**C**) stimulation for 30 min. (−), No stimulation.

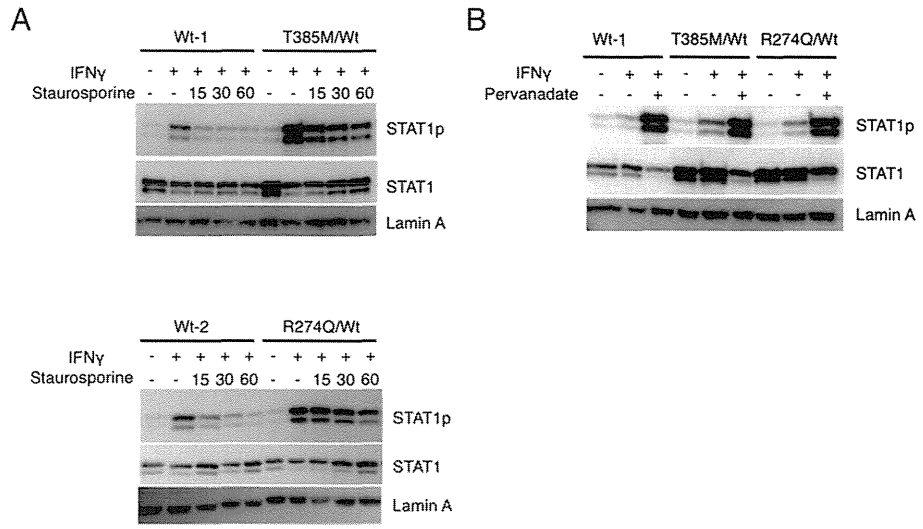

FIGURE 4. T385M was associated with hyperphosphorylation of STAT1 due to impaired dephosphorylation. (**A**) STAT1p expression in EBV-LCLs stimulated with IFN-γ for 30 min and then incubated with 1 μM staurosporine for 15, 30, or 60 min. (**B**) STAT1p expression in EBV-LCLs treated with pervanadate for 5 min and then stimulated with IFN-γ for 30 min.

to β-D-glucan stimulation with Curdlan (data not shown), indicating that the base change of c.661G>A, p.K221E in *CARD9* is not a disease-causing mutation but a single nucleotide polymorphism. The rest of the genes studied were demonstrated to be normal in both patients.

T385M is associated with gain of STAT1 function

Gain-of-function mutations in *STAT1* were very recently shown to be the genetic cause of autosomal-dominant or sporadic CMC (4–6). The reported mutations have been exclusively localized in the CC domain, leading to gain of STAT1 function due to impaired STAT1 dephosphorylation (4). To study whether the base change of c.1153C>T, p.T385M affecting the DBD of STAT1 also leads to gain of STAT1 function, the production of the downstream target of STAT1, IP-10, was studied following IFN-γ stimulation. IP-10 production was significantly higher in monocyte-derived macrophages from Patient 1 (T385M/Wt) and Patient 3 (R274Q/Wt) than in the matched control macrophages after IFN-γ–LPS stimulation (Fig. 2A). IP-10 production was also significantly higher in EBV-LCLs from Patient 1 (T385M/Wt) and Patient 3 (R274Q/Wt) after IFN-γ stimulation (Fig. 2B). These results indicated that T385M is a mutation leading to gain of STAT1 function.

STAT1 T385M leads to STAT1 hyperphosphorylation in response to IFN-γ, IFN-α, and IL-27 stimulation, which is due to impaired dephosphorylation

We then studied the STAT1 phosphorylation state in EBV-LCLs to determine the mechanisms of the gain of STAT1 function. Expression of phosphorylated STAT1 (STAT1p) protein following IFN-γ stimulation was higher in T385M/Wt and R274Q/Wt EBV-LCLs than in Wt EBV-LCLs (Fig. 3A). The hyperphosphorylated state of STAT1 was also observed following stimulation with IFN-α and IL-27 (Fig. 3B, 3C). Additionally, expression of total STAT1 in nuclear extract tends to be higher in T385M/Wt and R274Q/Wt EBV-LCLs than in Wt EBV-LCLs, especially without stimulation (Fig. 3). The mechanisms underlying STAT1 hyperphosphorylation in T385M/Wt EBV-LCLs were further explored with the tyrosine kinase inhibitor staurosporine and the phosphatase inhibitor pervanadate. The dephosphorylation of IFN-γ–ac-

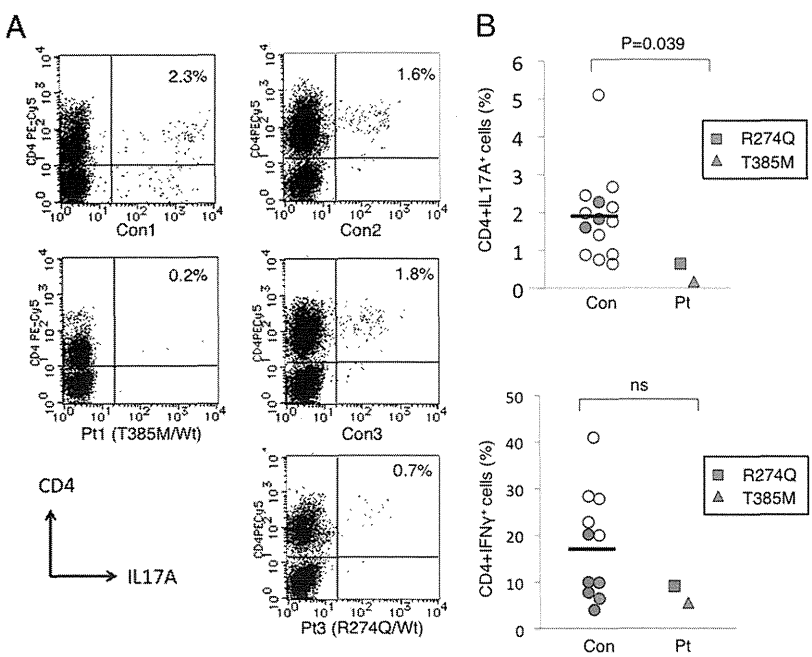

FIGURE 5. Patients 1 and 3 had deficient $CD4^+IL\text{-}17A^+$ cells but normal $CD4^+IFN\text{-}\gamma^+$ cells in response to PMA plus ionomycin stimulation. (**A**) Flow cytometric analysis of intracellular IL-17A expression following PMA plus ionomycin stimulation for 6 h. The proportion of $CD4^+IL\text{-}17A^+$ cells among $CD4^+$ cells was shown. (**B**) The proportion of $CD4^+IL\text{-}17A^+$ cells and $CD4^+IFN\text{-}\gamma^+$ cells among $CD4^+$ cells in normal controls and the patients. The horizontal lines indicate the mean proportion of $CD4^+IL\text{-}17A^+$ cells or $CD4^+IFN\text{-}\gamma^+$ cells in controls. Red and blue circles indicate controls obtained and analyzed at the same time as Patients 1 and 3, respectively. The *p* value was estimated using the Mann–Whitney *U* test. Con1, Control for Patient 1 obtained and analyzed at the same time; Con2 and Con3, controls for Patient 3 obtained and analyzed at the same time; Pt1, Patient 1; Pt3, Patient 3.

tivated T385M/Wt EBV-LCLs was impaired in the presence of staurosporine, as observed in R274Q/Wt EBV-LCLs (Fig. 4A). In contrast, with pervanadate treatment, the phosphorylation of STAT1 in T385M/Wt EBV-LCLs was similar to that seen in Wt EBV-LCLs (Fig. 4B). Therefore, the mechanisms underlying STAT1 hyperphosphorylation in T385M/Wt EBV-LCLs involve impaired dephosphorylation of STAT1, as observed in R274Q/Wt EBV-LCLs.

Patient 1 with the heterozygous T385M mutation in STAT1 had deficient Th17 cells

Deficient development of Th17 cells was documented to be associated with the development of CMC. CMC patients with gain-of-function mutations of *STAT1* affecting the CC domain have shown this defect (4). Therefore, we studied the proportion of $CD4^+IL\text{-}17A^+$ cells among $CD4^+$ cells in our patients after PMA plus ionomycin stimulation for 6 h. We also studied the population of $CD4^+IFN\text{-}\gamma^+$ cells to evaluate Th1 development. Patient 1 with the heterozygous T385M/Wt mutation of *STAT1* was reproducibly demonstrated to have dramatically reduced $CD4^+IL\text{-}17A^+$ cells (0.2% of $CD4^+$ cells), and Patient 3 with the heterozygous R274Q mutation had significantly reduced, but a little higher, $CD4^+IL\text{-}17A^+$ cells (0.7% of $CD4^+$ cells) (Fig. 5). The p value estimated using the Mann–Whitney U test was 0.039 between controls and the two patients. In contrast, both patients and controls had comparable percentages of $CD4^+IFN\text{-}\gamma^+$ cells (Fig. 5).

Discussion

To our knowledge, this study shows for the first time that the de novo heterozygous mutation of c.1153C>T in exon 14 (p.T385M), affecting the DBD of STAT1, is the genetic cause of sporadic CMC in two unrelated Japanese patients. The underlying mechanisms involve gain of STAT1 function due to impaired STAT1 dephosphorylation, as observed in the CC domain mutations (4).

Recent extensive studies of the STAT1 molecule reveal the association between the mutations affecting DBD and gain of STAT1 function. Based on crystallographic analysis, Darnell's group (7, 8) proposed a model of reorientation of phosphorylated "parallel" STAT1 dimers to an "antiparallel" form after leaving the DNA, which allows for reciprocal association of the CC domain and a pocket residue of the DBD for dephosphorylation. They further demonstrated in direct mutagenesis experiments that mutations of the pocket residues of the DBD, Q340A or Q340W, G384A or G384W, and Q408A or Q408W, resulted in impaired dephosphorylation of STAT1 (8). The fact that T385, the amino acid altered in two of our patients, is evolutionarily conserved and is positioned next to the pocket residue G384 may indicate that it is also critical in the reciprocal association with the CC domain for stabilizing the antiparallel structure and for dephosphorylation. It is also possible that this mutation of the DBD leads to impaired dissociation from the DNA, which may also cause a resistance to dephosphorylation of the STAT1 molecule. Higher expression of total STAT1 in nuclear extracts from T385M/Wt and R274Q/Wt EBV-LCLs than from Wt EBV-LCLs may reflect impaired nuclear export due to a resistance to dephosphorylation of the mutant STAT1 molecule (18), although the precise mechanisms were not determined in this study.

There may be more patients with CMC who carry gain-of-function mutations affecting the DBD of STAT1, given that significant numbers of patients with *STAT1* mutations are reported from all over the world (4–6). Additionally, crystallographic analysis and mutagenesis studies showed that mutations in the N-terminal domain (aa 1–130) also resulted in persistent phosphorylation (7, 8). This suggests that mutations affecting the N-terminal domain may also be a genetic cause of CMC.

We demonstrated deficient Th17 cells (0.2% of $CD4^+$ cells) in Patient 1 with the heterozygous T385M mutation, which was similar to or more severe than the defect observed in Patient 3 with the heterozygous R274Q mutation (0.7% of $CD4^+$ cells). Deficient development of Th17 cells may explain the increased susceptibility to *Candida* infection. IFN-γ, IFN-α, and IL-27 are potent inhibitors of Th17 cell development via STAT1 in mice and/or humans (19–21). Therefore, gain of STAT1 function in response to IFN-γ, IFN-α, or IL-27, which was observed in our patients, could be associated with deficient Th17 cell development. However, it remains to be determined precisely how gain of STAT1 function leads to deficient Th17 cells.

It is unclear whether there are differences in the clinical spectrum or severity of the disease between patients with the DBD mutations and the CC domain mutations. It might be worth noting that the two patients with the DBD mutation of T385M developed bronchiectasis in their early childhood, and one of them eventually developed HLH; these have not been described in patients with CC domain mutations.

With regard to HLH, administration of an anti–IFN-γ Ab was recently shown to have a therapeutic effect in two murine models of human hereditary HLH: perforin-deficient and Rab27a-deficient mice (22). Careful evaluation of the results indicates that T385M could be associated with higher expression of STAT1p in response to various stimulations (Fig. 3). Therefore, CMC patients with the DBD mutation of T385M may be more susceptible to the conditions presumably associated with enhanced IFN-γ–STAT1 signals, such as HLH. Detailed investigations of the clinical spectrum of these two populations should be conducted.

Acknowledgments

We thank Dr. D.M. Stewart (Metabolism Branch, National Cancer Institute, National Institutes of Health, Bethesda, MD) for reviewing the manuscript, the patients and their families for participation in this study, and Dr. H. Kanegane (Department of Pediatrics, Graduate School of Medicine, University of Toyama, Toyama, Japan) for coordinating patient recruitment.

Disclosures

The authors have no financial conflicts of interest.

References

1. Kirkpatrick, C. H. 1994. Chronic mucocutaneous candidiasis. *J. Am. Acad. Dermatol.* 31: S14–S17.
2. Mathis, D., and C. Benoist. 2009. Aire. *Annu. Rev. Immunol.* 27: 287–312.
3. Coleman, R., and R. J. Hay. 1997. Chronic mucocutaneous candidosis associated with hypothyroidism: a distinct syndrome? *Br. J. Dermatol.* 136: 24–29.
4. Liu, L., S. Okada, X. F. Kong, A. Y. Kreins, S. Cypowyj, A. Abhyankar, J. Toubiana, Y. Itan, M. Audry, P. Nitschke, et al. 2011. Gain-of-function human STAT1 mutations impair IL-17 immunity and underlie chronic mucocutaneous candidiasis. *J. Exp. Med.* 208: 1635–1648.
5. van de Veerdonk, F. L., T. S. Plantinga, A. Hoischen, S. P. Smeekens, L. A. Joosten, C. Gilissen, P. Arts, D. C. Rosentul, A. J. Carmichael, C. A. Smits-van der Graaf, et al. 2011. STAT1 mutations in autosomal dominant chronic mucocutaneous candidiasis. *N. Engl. J. Med.* 365: 54–61.
6. Smeekens, S. P., T. S. Plantinga, F. L. van de Veerdonk, B. Heinhuis, A. Hoischen, L. A. Joosten, P. D. Arkwright, A. Gennery, B. J. Kullberg, J. A. Veltman, et al. 2011. STAT1 hyperphosphorylation and defective IL12R/IL23R signaling underlie defective immunity in autosomal dominant chronic mucocutaneous candidiasis. *PLoS ONE* 6: e29248.
7. Zhong, M., M. A. Henriksen, K. Takeuchi, O. Schaefer, B. Liu, J. ten Hoeve, Z. Ren, X. Mao, X. Chen, K. Shuai, and J. E. Darnell, Jr. 2005. Implications of an antiparallel dimeric structure of nonphosphorylated STAT1 for the activation-inactivation cycle. *Proc. Natl. Acad. Sci. USA* 102: 3966–3971.
8. Mertens, C., M. Zhong, R. Krishnaraj, W. Zou, X. Chen, and J. E. Darnell, Jr. 2006. Dephosphorylation of phosphotyrosine on STAT1 dimers requires extensive spatial reorientation of the monomers facilitated by the N-terminal domain. *Genes Dev.* 20: 3372–3381.
9. Nagashima, T., A. Miyanoshita, Y. Sakiyama, Y. Ozaki, A. C. Stan, and K. Nagashima. 2000. Cerebral vasculitis in chronic mucocutaneous candidiasis: autopsy case report. *Neuropathology* 20: 309–314.

10. Yamada, M., Y. Okura, Y. Suzuki, S. Fukumura, T. Miyazaki, H. Ikeda, S. I. Takezaki, N. Kawamura, I. Kobayashi, and T. Ariga. 2012. Somatic mosaicism in two unrelated patients with X-linked chronic granulomatous disease characterized by the presence of a small population of normal cells. *Gene* 497: 110–115.
11. Schreiber, E., P. Matthias, M. M. Müller, and W. Schaffner. 1989. Rapid detection of octamer binding proteins with 'mini-extracts', prepared from a small number of cells. *Nucleic Acids Res.* 17: 6419.
12. Nagamine, K., P. Peterson, H. S. Scott, J. Kudoh, S. Minoshima, M. Heino, K. J. Krohn, M. D. Lalioti, P. E. Mullis, S. E. Antonarakis, et al. 1997. Positional cloning of the APECED gene. *Nat. Genet.* 17: 393–398.
13. Finnish-German APECED Consortium. 1997. An autoimmune disease, APECED, caused by mutations in a novel gene featuring two PHD-type zinc-finger domains. *Nat. Genet.* 17: 399–403.
14. Ferwerda, B., G. Ferwerda, T. S. Plantinga, J. A. Willment, A. B. van Spriel, H. Venselaar, C. C. Elbers, M. D. Johnson, A. Cambi, C. Huysamen, et al. 2009. Human dectin-1 deficiency and mucocutaneous fungal infections. *N. Engl. J. Med.* 361: 1760–1767.
15. Glocker, E. O., A. Hennigs, M. Nabavi, A. A. Schäffer, C. Woellner, U. Salzer, D. Pfeifer, H. Veelken, K. Warnatz, F. Tahami, et al. 2009. A homozygous CARD9 mutation in a family with susceptibility to fungal infections. *N. Engl. J. Med.* 361: 1727–1735.
16. Puel, A., S. Cypowyj, J. Bustamante, J. F. Wright, L. Liu, H. K. Lim, M. Migaud, L. Israel, M. Chrabieh, M. Audry, et al. 2011. Chronic mucocutaneous candidiasis in humans with inborn errors of interleukin-17 immunity. *Science* 332: 65–68.
17. Sharfe, N., H. K. Dadi, M. Shahar, and C. M. Roifman. 1997. Human immune disorder arising from mutation of the alpha chain of the interleukin-2 receptor. *Proc. Natl. Acad. Sci. USA* 94: 3168–3171.
18. McBride, K. M., C. McDonald, and N. C. Reich. 2000. Nuclear export signal located within theDNA-binding domain of the STAT1transcription factor. *EMBO J.* 19: 6196–6206.
19. Villarino, A. V., E. Gallo, and A. K. Abbas. 2010. STAT1-activating cytokines limit Th17 responses through both T-bet-dependent and -independent mechanisms. *J. Immunol.* 185: 6461–6471.
20. Ramgolam, V. S., Y. Sha, J. Jin, X. Zhang, and S. Markovic-Plese. 2009. IFN-beta inhibits human Th17 cell differentiation. *J. Immunol.* 183: 5418–5427.
21. Diveu, C., M. J. McGeachy, K. Boniface, J. S. Stumhofer, M. Sathe, B. Joyce-Shaikh, Y. Chen, C. M. Tato, T. K. McClanahan, R. de Waal Malefyt, et al. 2009. IL-27 blocks RORc expression to inhibit lineage commitment of Th17 cells. *J. Immunol.* 182: 5748–5756.
22. Pachlopnik Schmid, J., C. H. Ho, F. Chrétien, J. M. Lefebvre, G. Pivert, M. Kosco-Vilbois, W. Ferlin, F. Geissmann, A. Fischer, and G. de Saint Basile. 2009. Neutralization of IFNgamma defeats haemophagocytosis in LCMV-infected perforin- and Rab27a-deficient mice. *EMBO. Mol. Med.* 1: 112–124.

Process for immune defect and chromosomal translocation during early thymocyte development lacking ATM

Takeshi Isoda,[1] Masatoshi Takagi,[1] Jinhua Piao,[1] Shun Nakagama,[1] Masaki Sato,[1] Kyoko Masuda,[2] Tomokatsu Ikawa,[2] Miyuki Azuma,[3] Tomohiro Morio,[1] Hiroshi Kawamoto,[2] and Shuki Mizutani[1]

[1]Department of Pediatrics and Developmental Biology, Graduate School of Medicine, Tokyo Medical and Dental University, Tokyo, Japan; [2]Laboratory for Lymphocyte Development, RIKEN Research Centre for Allergy and Immunology, Tokyo, Japan; and [3]Department of Molecular Immunology, Tokyo Medical and Dental University, Tokyo, Japan

Immune defect in ataxia telangiectasia patients has been attributed to either the failure of V(D)J recombination or class-switch recombination, and the chromosomal translocation in their lymphoma often involves the TCR gene. The ATM-deficient mouse exhibits fewer CD4 and CD8 single-positive T cells because of a failure to develop from the $CD4^+CD8^+$ double-positive phase to the single-positive phase. Although the occurrence of chromosome 14 translocations involving TCR-δ gene in ATM-deficient lymphomas suggests that these are early events in T-cell development, a thorough analysis focusing on early T-cell development has never been performed. Here we demonstrate that ATM-deficient mouse thymocytes are perturbed in passing through the β- or γδ-selection checkpoint, leading in part to the developmental failure of T cells. Detailed karyotype analysis using the in vitro thymocyte development system revealed that RAG-mediated TCR-α/δ locus breaks occur and are left unrepaired during the troublesome β- or γδ-selection checkpoints. By getting through these selection checkpoints, some of the clones with random or nonrandom chromosomal translocations involving TCR-α/δ locus are selected and accumulate. Thus, our study visualized the first step of multistep evolutions toward lymphomagenesis in ATM-deficient thymocytes associated with T-lymphopenia and immunodeficiency. (*Blood*. 2012;120(4):789-799)

Introduction

Ataxia telangiectasia (AT) is an autosomal recessive disorder that is characterized by cerebellar ataxia, telangiectasia, immune defects, and a predisposition to malignancy, particularly leukemia/lymphoma.[1-4] The immune defects observed in AT patients include fewer than normal T and B lymphocytes and lower serum IgA, IgG2, and IgE levels.[5,6] The ATM knockout ($ATM^{-/-}$) mouse has fewer CD4 and CD8 single-positive (SP) T cells because of a failure to develop from the $CD4^+CD8^+$ double-positive (DP) phase to the SP phase has been noted.[7-9]

The responsible gene ATM works as a master regulator for maintaining DNA integrity and has crucial role for responding DNA double-strand break (DSB) from extrinsic and intrinsic factors, such as ionizing radiation, free oxygen radicals, unscheduled replicative stimuli, and DSB during V(D)J recombination.[1-4,10] The role of ATM for V(D)J recombination of lymphocyte antigen receptor gene assembly or immunoglobulin synthesis is relatively well characterized. V(D)J recombination is initiated by the recombination activating genes (RAG)1 and RAG2 endonuclease. RAG protein binds and cleaves the DNA at specific recombination signal sequences (RSSs) that flank each V, D, and J gene segment.[11] After cleavage, ATM and other DNA damage response proteins, such as NBS1, 53BP1, and phosphorylated H2AX localize to DSBs.[12] Concurrently, classic nonhomologous end-joining complex is recruited.[13] Recruitment of these molecules functions directly in the repair of chromosomal DNA DSBs by maintaining DNA ends in repair complexes. These processes promote correct resolution of inversional V(D)J recombination and prevent aberrant antigen receptor locus translocations.[14] ATM deficiency leads to inefficient coding end binding after the RAG-dependent DSB generation at immunoglobulin and T-cell antigen receptor loci.[15] Transition failure from DP to SP observed in $ATM^{-/-}$ mice has been explained because of decreased efficiency in V-J rearrangement of the T-cell receptor (*Tcr*) α locus, accompanied by increased frequency of unresolved *TcrJα* coding end breaks.[8,9]

Most of thymic lymphomas observed in ATM knockout mouse recapitulate these aspects of human AT and possess chromosome 14 translocations at the *Tcrα/δ* locus preferentially with chromosome 12 where mouse *BCL11b* gene located, and mostly express $CD4^+CD8^+$ phenotype.[7,16] Interestingly, recent finding revealed that recurrent chromosome 14 translocations observed in ATM-deficient thymic lymphomas are associated with V(D)J recombination errors at *Tcrδ*, as opposed to *Tcrα* locus. In addition, *Eα* is completely dispensable for the oncogenic processes leading to these tumors.[17]

During T-cell development, early T-cell precursors differentiate first into $CD4^-CD8^-$ double-negative (DN) and then to DP stages. $CD4^-CD8^-$ DN T-cell subsets are further subdivided into DN1 to DN4 based on their expression of CD25 and CD117.[18] Rearrangement of TCR-β, -γ, and -δ genes occurs mainly at the DN3 stage, although TCR-δ and -γ genes are thought to be partially rearranged at DN1 and DN2 stages. Successful rearrangement of TCR genes in DN3 cells drives their further differentiation. DN3 stage is subdivided into DN3a and DN3b depending on the successful TCR-β rearrangement, which is followed by the DN4 stage.[19]

Submitted February 26, 2012; accepted June 6, 2012. Prepublished online as *Blood* First Edition paper, June 18, 2012; DOI 10.1182/blood-2012-02-413195.

The online version of this article contains a data supplement.

The publication costs of this article were defrayed in part by page charge payment. Therefore, and solely to indicate this fact, this article is hereby marked "advertisement" in accordance with 18 USC section 1734.

It has been speculated that immunodeficiency and susceptibility to lymphoma in AT are the result of a defective TCR recombination and/or class switch recombination. Although the chromosome 14 translocations involving the breaks at TCR-δ locus in ATM-deficient T cells suggest these to be early events in T-cell development, in-depth analyses focusing on early T-cell development at DN phase has not been elucidated. Here we show that ATM-deficient thymocytes fail to progress from DN3a to DN3b, and chromosome 14 breaks and translocations involving TCR-α/δ locus concurrently occur during this transitional stage.

Methods

Mice

$ATM^{+/-}$ mice, originally on the129SvJ × C57BL/6 background, were a kind gift from Dr P. J. McKinnon (St Jude Children's Research Hospital, Memphis, TN).[20] The $ATM^{+/-}$ mice were backcrossed for more than 15 generations with C57BL/6 mice. $ATM^{+/+}$ and $ATM^{-/-}$ mice were analyzed at 6 to 10 weeks of age. The *Atm* genotype was confirmed by PCR using tail DNA. $RAG2^{-/-}$ mice (BALB/c) and congenic CD45.1 mice (C57BL/6) were obtained from The Jackson Laboratory. The $RAG2^{-/-}$ mice were backcrossed with C57BL/6 mice. To generate mice deficient for both RAG2 and ATM, $RAG2^{-/-}$ and $ATM^{+/-}$ mice were crossed and the progeny were typed by PCR. All of the mice were bred in the specific pathogen-free unit in the vivarium in Tokyo Medical and Dental University. Animal care was approved by the Animal Care and Use Committee (protocol no. 0120228B). Sterile anti-CD3ϵ mAb (145-2C11) was injected intraperitoneally (150 μg/mouse).

Antibodies, flow cytometry, sorting, intracellular staining, and apoptosis analysis

Samples from thymi or cultured cells were stained using 5 or 6 antibody color combinations. The data were acquired on a FACSCalibur or FACSAria II (BD Biosciences) flow cytometry and analyzed using CellQuest Version 3.3 or FACSDIVA software. Each differential thymocyte phase was sorted by FACSAria II Version 6.1.3 (BD Biosciences) with more than 99% purity. The following antibodies were purchased from BD Biosciences: anti–mouse CD3ϵ NA/LE, PE/Cy7 (145-2C11), CD25 PE, PE/Cy7 (PC61), CD27 PE (LG.3A10), CD44 APC (IM7), CD45 PE/Cy5, PE/Cy7 (30-F11), CD117 APC (2B8), γδ T-cell receptor PE (GL3), TCR-β chain FITC (H57-597), 7-amino-actinomycin D, annexin V, CD3 molecular complex FITC (17A2), CD4 FITC (RM4-5), CD8a FITC, PE (53-6.7), CD11b FITC (M1/70), TER-119 FITC (TER-119), Gr-1 FITC (RB6-8C5), CD19 FITC (1D3), B220 FITC (RA3-6B2), and NK1.1 FITC (PK136). The following antibodies were purchased from BioLegend: CD27 PerCP/Cy5.5 (LG.3A10), CD45.1 PE/Cy7 (A20), CD45.2 APC/Cy7, (104) CD117 APC/Cy7 (2B8), γδ T-cell receptor APC (GL3), TCR-β chain PerCP/Cy5.5, and APC-Cy7 (H57-597). The phospho-histone H2A.X (Ser139) Alexa-647 (20E3) antibody was purchased from Cell Signaling. The following were used as lineage markers: CD3, CD4, CD8, CD19, B220, $CD11b^{-}$, Gr1, NK1.1, and TER119. We measured intracellular TCR-β, TCR-γδ and pH2AX by flow cytometry using the IntraPrep Kit (Beckman Coulter). For apoptosis analysis, the cells were stained with the surface marker for 15 minutes, washed in 1% BSA containing PBS, and then stained with annexin V and 7-amino-actinomycin D in annexin V binding buffer according to the manufacturer's instructions (BD Biosciences).

Cell-cycle analysis

We used Click-iT EdU flow cytometry assay kits for cell-cycle analysis (Invitrogen). The mice were injected intraperitoneally with 100 μg of EdU in PBS. After 3 hours, single-cell suspensions were prepared from thymi and stained for cell surface markers. DN2, DN3a, DN3b, and DP stage thymocytes were all sorted by FACSAria II. The sorted cells were subjected to EdU detection according to the protocol of the manufacturer and analyzed with the FACSCalibur.

PCR detection for TCR-β V(D)J and DJ rearrangement

TCR gene rearrangement was analyzed as previously described.[21] Genomic DNA was extracted from each thymocyte differentiation stage using a QIAamp DNA blood mini-kit (QIAGEN). The reaction volume was 25 μL and contained 10 ng of genomic DNA, 2.5 μL of 10× PCR buffer, 4 μL of 2.5mM dNTPs, 2.5 μL of 25μM $MgCl_2$, 0.4μM of each primer, and 2.5 U of LA Taq polymerase (TaKaRa Biotechnology). The PCR reactions were performed as follows: 5 minutes at 95°C followed by 33 to 35 cycles of 30 seconds at 95°C, 30 seconds at 60°C, and 2 minutes at 68°C, and a final extension for 7 minutes at 72°C with the GeneAmp PCR System 9700 (Applied Biosystems). The PCR products were analyzed on agarose gels stained with ethidium bromide.

Real-time PCR

Total RNA was isolated from DN2, DN3a, DN3b, DN4, and DP cells using an RNeasy kit (QIAGEN). cDNA was synthesized using Superscript III (Invitrogen) according to the protocol of the manufacturer. Real-time PCR was performed using SYBR Green, and the reactions were monitored using a LightCycler 480 (Roche Diagnostics). The reactions were performed in duplicate at 95°C for 5 minutes for denaturation followed by 40 cycles of 95°C for 10 seconds, 60°C for 10 seconds, and 72°C for 10 seconds. The primer sequences used are those described previously for pre–TCR-α,[22] BCL11b,[23] RAG1, and RAG2.[24]

Growth factors

Recombinant murine stem cell factor, recombinant murine FMS-like tyrosine kinase ligand (Flt3L), and rmIL-7 were purchased from R&D Systems.

Isolation of adult long-term repopulating hematopoietic stem cells

Single-cell suspensions of BM cells were prepared from 4- to 8-week-old mice. The cells were incubated with anti-Sca1 and anti-CD105 mAbs for 15 minutes on ice. Next, MACS magnetic beads were used for $Sca1^{+}$ and $CD105^{+}$ enrichment in a 2-step process according to the protocol of the manufacturer (Miltenyi Biotec).

In vitro differentiation of long-term repopulating hematopoietic stem cells

We cultured OP9-DLL1 cells in a 10-cm or 6-well plate with α-MEM medium containing 20% FBS, streptomycin (100 mg/mL), and penicillin (100 U/mL) at 37°C in a humidified atmosphere containing 5% CO_2. Approximately 1 to 3 × 10^4 long-term repopulating hematopoietic stem cells per well were cultured on semiconfluent OP9-DLL1 cells in medium containing 5 ng/mL of Flt3L and 1 ng/mL of IL-7. Floating cells were transferred to a fresh monolayer of semiconfluent OP9-DLL1 cells on days 6, 10, 14, and 18. For *N*-acetyl-*L*-cysteine (NAC) experiments, the cells were incubated with 100μM or1mM NAC (Sigma-Aldrich). Singly sorted DN3a and DN3b cells from WT and $ATM^{-/-}$ thyme were cultured on OP9-DLL1 cells containing 5 ng/mL Flt3L and 1 ng/mL IL-7 in 96-well plates.

Bone marrow transplantation

Recipient mice (CD45.1) received myeloablative conditioning with 10 Gy of total body irradiation 6 hours before bone marrow transplantation (BMT). Bone marrow cells were harvested from donor mice (CD45.2) on the day of BMT and injected (1 × 10^7cells) into the tail vein of recipient mice. The mice received ad libitum drinking water containing 1 mg/mL neomycin trisulphate salt hydrate (Sigma-Aldrich) and 100 U/mL polymyxin B sulfate salt (Sigma-Aldrich).

FISH analysis of chromosome 12, chromosome 14, and the TCR-α/δ locus in DN phase thymocytes

To obtain DN2/DN3a cells, long-term repopulating hematopoietic stem cells were cultured on OP9-DLL1 cells in α-MEM containing 20% FBS, streptomycin (100 mg/mL), penicillin (100 U/mL), and 10 ng/mL of Flt3L, IL-7, and stem cell factor. To generate metaphase spreads, day 15 to 17 DN2/DN3a cells were treated with 25 ng/mL colcemid (Sigma-Aldrich) for 2 hours. To collect DN3b/DN4 cells, we continued to cultivate differentiated DN2/DN3a cells in the same medium, but containing 5 ng/mL Flt3L and 1 ng/mL IL-7 for 7 to 10 additional days. After 25 ng/mL colcemid treatment for 2 hours, the DN3b/DN4 cells were sorted using a FACSAria II. DN2/DN3a cells and DN3b/DN4 cells were treated in hypotonic solution containing 0.06M potassium chloride and 0.02% sodium citrate solution for 20 minutes and then fixed in methanol and acetic acid. To perform FISH assays for the TCR-α/δ locus breaks, we used BAC probes for the 5′-end (RP23-204N18; 5′; blue) and 3′-end (RP23-10K20; green) of the TCR-α/δ locus. The BACs were labeled by amine-nick translation using the FISH Tag DNA multicolor kit according to the manufacturer's protocol (Invitrogen). Chromosome 12 (green) and 14 (red) paint probes were purchased from Applied Spectral Imaging. The painting probes (10 μL) were mixed with 100 ng of 5′- and 3′-TCR α/δ locus probes and denatured at 80°C for 10 minutes before use. The slides were denatured at 67°C for 90 seconds and dehydrated in a cold ethanol series of 70%, 90%, and 100%. Hybridization was performed for 20 hours in a humidified chamber at 37°C. The slides were stringently washed in 0.4 × saline sodium citrate at 73°C for 4.5 minutes followed by 4 × saline sodium citrate/0.1% Tween-20 for 2 minutes and then mounted in SlowFade Gold antifade reagent (Invitrogen) with 4,6-diamidino-2-phenylindole (Vector Laboratories). Images were captured with an FV10i confocal microscope (Olympus). Image acquisition and processing were performed using an Olympus FluoView Version 3.0 Viewer (Olympus).

Data analysis

Data are expressed as mean plus or minus SE. Unpaired *t* tests or ANOVA were used for statistical analysis. *P* values less than .05 were considered significant.

Results

Impaired development from DN3a to DN3b in ATM $^{-/-}$ thymus in vivo

Consistent with previous reports,[8,9] the proportion of CD4SP and CD8SP cells was decreased (Figure 1A) and total thymocyte numbers were significantly reduced in ATM$^{-/-}$ mice (Figure 1B). The relative percentage of cells in the DN phase was significantly higher in ATM$^{-/-}$ than in ATM$^{+/+}$ mice (Figure 1C); and although the relative percentage of cells in DN1 and DN2 was slightly lower in total thymocytes of ATM knockout mice, there was an accumulation of cells in DN3 (Figure 1D-E). Interestingly, DN3b cells, which are characterized by the expression of CD27 and intracellular TCR-β or TCR-γδ, were significantly reduced in ATM$^{-/-}$ mice (Figure 1F-I). Collectively, these data indicate that ATM-deficient thymocytes fail to transit from the DN3a to the DN3b stage in both γδ T-cell and αβ T-cell lineages in vivo.

Transition failure from DN3a to DN3b of ATM$^{-/-}$ thymocyte in vitro

To further evaluate the failure in transition from DN3a to DN3b, we took advantage of an in vitro thymocyte development system. CD105^{+}Sca-1^{+} BM cells, which represent a progenitor population containing hematopoietic stem cells (hereafter referred to as BM progenitors), from ATM$^{+/+}$ and ATM$^{-/-}$ mice were cocultured on OP9-Delta like 1 (DLL1) cells with Flt3L and IL-7.[25] DP cells began to appear on day 10 in ATM$^{+/+}$ cell cultures and gradually accumulated. By contrast, DP cell production was not seen until day 14 in the ATM$^{-/-}$ cultures (Figure 2A-B). The DN phase profile gated on a lineage-negative fraction showed a failure in transition from DN3 to DN4 for the ATM$^{-/-}$ BM progenitors (Figure 2C-D). Analysis of intracellular (ic) TCR-β expression in the ATM$^{-/-}$ DN3 population allowed us to focus on the defect in the transition from the DN3a to the DN3b stage (Figure 2E-F). Neither T-cell development nor the transition from DN3a to DN3b in ATM$^{-/-}$ BM progenitors was restored by the treatment with 100μM or 1mM antioxidant NAC (supplemental Figures 1-3, available on the *Blood* Web site; see the Supplemental Materials link at the top of the online article), ruling out the possibility that oxidative stress is involved in these processes, which was in contrast to the previous findings in the maintenance of HSCs and T-cell development.[26,27] To directly demonstrate that the developmental failure of T cells in ATM$^{-/-}$ lies in the transition from DN3a to DN3b, singly sorted DN3a and DN3b cells of wild-type and knockout mice were cultured on OP9-DLL1 and analyzed for their potential to differentiate into DP cells. These clonal assays also confirmed that the DN3a stage cells fail to transit to DP cells in ATM$^{-/-}$ cells (10% ± 0.78% frequency) compared with ATM$^{+/+}$ cells (34.2% ± 4.59% frequency). However, ATM$^{-/-}$ DN3b cells differentiated into DP cells as efficiently as the ATM$^{+/+}$ cells (Figure 2G). Thus, the in vivo transitional failure from DN3a to DN3b was recapitulated in an in vitro system.

Inefficient TCR-γδ lineage differentiation in ATM$^{-/-}$ mice

The ratio of peripheral TCR-γδ to TCR-αβ T cells (TCR-γδ/TCR-αβ) in AT patients is reportedly relatively higher.[28] Consistent with previous reports, the TCR-γδ cell population was relatively higher in ATM$^{-/-}$ mice thymus (Figure 3A). However, the absolute number of TCR-β and TCR-γδ–positive cells was significantly decreased in ATM$^{-/-}$ thymus than ATM$^{+/+}$ thymus (Figure 3B). Then, in vitro T-cell differentiation system using BM progenitors was used to determine how cell surface TCR-β and γδ expression is deregulated in ATM$^{-/-}$ cells, as reflected by the delay or decrease in numbers of TCR-γδ and TCR-β T cells (Figure 3C-D). Possible involvement of reactive oxygen species was evaluated by NAC treatment, and NAC was shown not to improve the failure of TCR-β and TCR-γδ expression in ATM$^{-/-}$ thymocytes (supplemental Figure 4A-B). Thus, γδ-TCR lineage development is also affected in ATM$^{-/-}$ mice, but this was not reactive oxygen species dependent.

ATM is not involved in differentiation program from DN3 to DP

To confirm that the developmental program occurring from DN3b to DP stages is intact, we examined T-cell development in RAG2$^{-/-}$ mice. In both ATM$^{+/+}$RAG2$^{-/-}$ and ATM$^{-/-}$RAG2$^{-/-}$ mice, thymocytes accumulated equally at the DN3 stage, indicating that ATM has no effect on the development up to the β-selection checkpoint (supplemental Figure 5A), which is the gatekeeper for cells with a functional TCR-β chain. The developmental arrest at DN3 in RAG2$^{-/-}$ mice can be bypassed by stimulation of the pre-TCR complex (TCR-β/pTα/CD3) with anti-CD3ε antibody, allowing one to analyze the integrity of this signaling pathway in cell differentiation.[29] By anti-CD3ε stimulation, thymocytes from ATM$^{-/-}$RAG2$^{-/-}$ mice arrested at the DN3 stage differentiated into the DP stage as efficiently as those from ATM$^{+/+}$RAG2$^{-/-}$ mice, and there was no difference in cell expansion efficiency

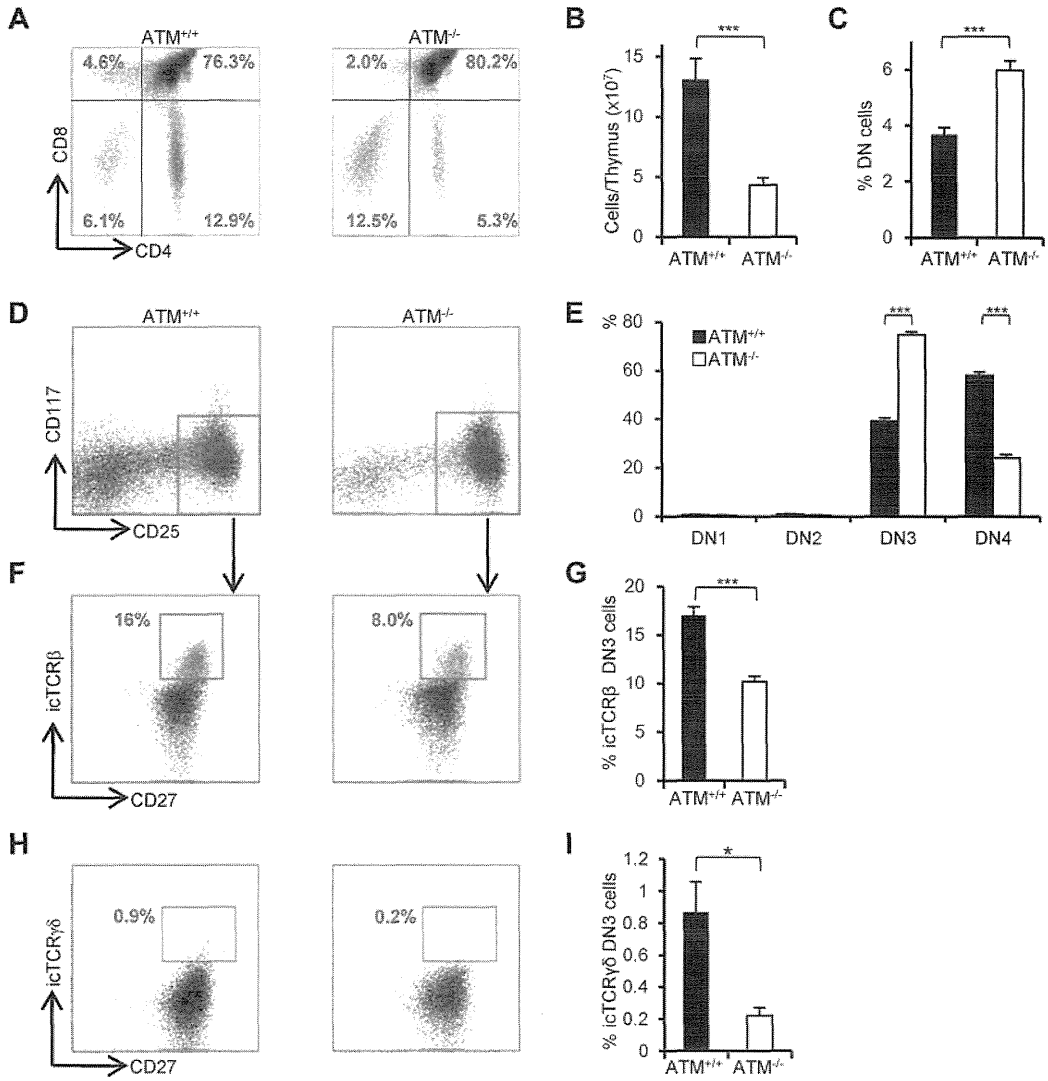

Figure 1. Developmental failure at the transition step from DN3a to DN3b in ATM$^{-/-}$ thymocytes. (A) Representative dot plots showing CD4 and CD8 profiles from ATM$^{+/+}$ and ATM$^{-/-}$ mice. (B) Absolute numbers of total thymocytes in ATM$^{+/+}$ and ATM$^{-/-}$ mice. (C) Relative percentage of lineage-negative cells. (D) Representative dot plots are gated on double-negative (DN) cells from ATM$^{+/+}$ and ATM$^{-/-}$ mice, when DN3 cells reached at 1 × 10^4 cells. Red dots indicate DN3b cells that are back-gated from CD27$^+$icTCR-β$^+$ fraction. (E) Bar graph represents DN1, DN2, DN3, and DN4 thymocyte percentages. (F) Dot plots are gated on DN3 cells (CD25 low, indicated in red in the top panels). DN3a cells are shown as CD27^{low} intracellular (ic) TCR-β$^-$. DN3b cells are CD27^{high}icTCR-β$^+$ and are indicated as red dots in red squares. (G) Bar graph represents icTCR-β–positive DN3b thymocyte percentages in the DN3 fraction. (A-G) The data were obtained from 12 ATM$^{+/+}$ mice and 11 ATM$^{-/-}$ mice at 4 to 8 weeks of age. (H) Dot plot data gated on DN3 cells from ATM$^{+/+}$ and ATM$^{-/-}$ mice. The icTCR-γδ–positive cells, which are indicated as red dots in the black squares, are CD27$^+$icTCR-γδ$^+$. (I) Percentages of icTCR-γδ–positive DN3b thymocytes in the DN3 fraction. (H-I) Data were obtained from 6 ATM$^{+/+}$ mice and 5 ATM$^{-/-}$ mice. Data are representative of at least 3 independent experiments (mean ± SE). *$P < .05$, ***$P < .001$.

(supplemental Figure 5B-C). We further examined the expression profiles of genes essential for early T-cell development, such as BCL11b, pTα, RAG1, and RAG2, in ATM$^{-/-}$ mouse thymocytes and found that they were normally expressed (supplemental Figure 6). These results indicate that the impaired development seen at the DN stage of ATM$^{-/-}$ thymocytes is not the result of the failure of the pre-TCR complex-dependent signaling pathway.

ATM-deficient thymic stroma supports normal transition from DN3a to DN3b

ATM-deficient thymic stromal cells reportedly do not affect the transition failure from DP to SP phase using BMT experiments.[30] Recent reports have identified a role for the stromal cell derived factor 1α and its receptor CXC chemokine receptor 4 in β-selection.[31,32] The functional role of ATM-deficient thymic stromal cells in β-selection of thymocytes has not been fully elucidated. To determine whether ATM-deficient thymic stromal cells affect thymocyte differentiation during DN phase, BM from ATM$^{+/+}$ and ATM$^{-/-}$ C57/BL6 Ly5.2 donors was transplanted into lethally irradiated wild-type ATM$^{+/+}$ C57/BL6 Ly5.1 recipients. Consistent with the result observed in ATM$^{-/-}$ mice, total thymocyte cellularity and absolute number of TCR-β and TCR-γδ T cells gated on CD45.2 were significantly reduced in the ATM$^{-/-}$ donor group (Figure 4A-C). ATM$^{-/-}$ thymocytes (CD45.2) in vivo reconstituted in the wild-type thymus also showed the transitional failure from DN3a to DN3b phase (Figure 4D-F). These findings of in vivo ATM$^{-/-}$ thymocyte differentiation in the thymic environment of ATM$^{+/+}$ C57/BL6 Ly5.1 corresponded well to the findings in those cultured on OP9-DLL1 in vitro (Figure 2E-F). These results ruled out the possibility that differentiation defect of thymocytes at β-selection checkpoint is caused by thymic environment in the absence of ATM.

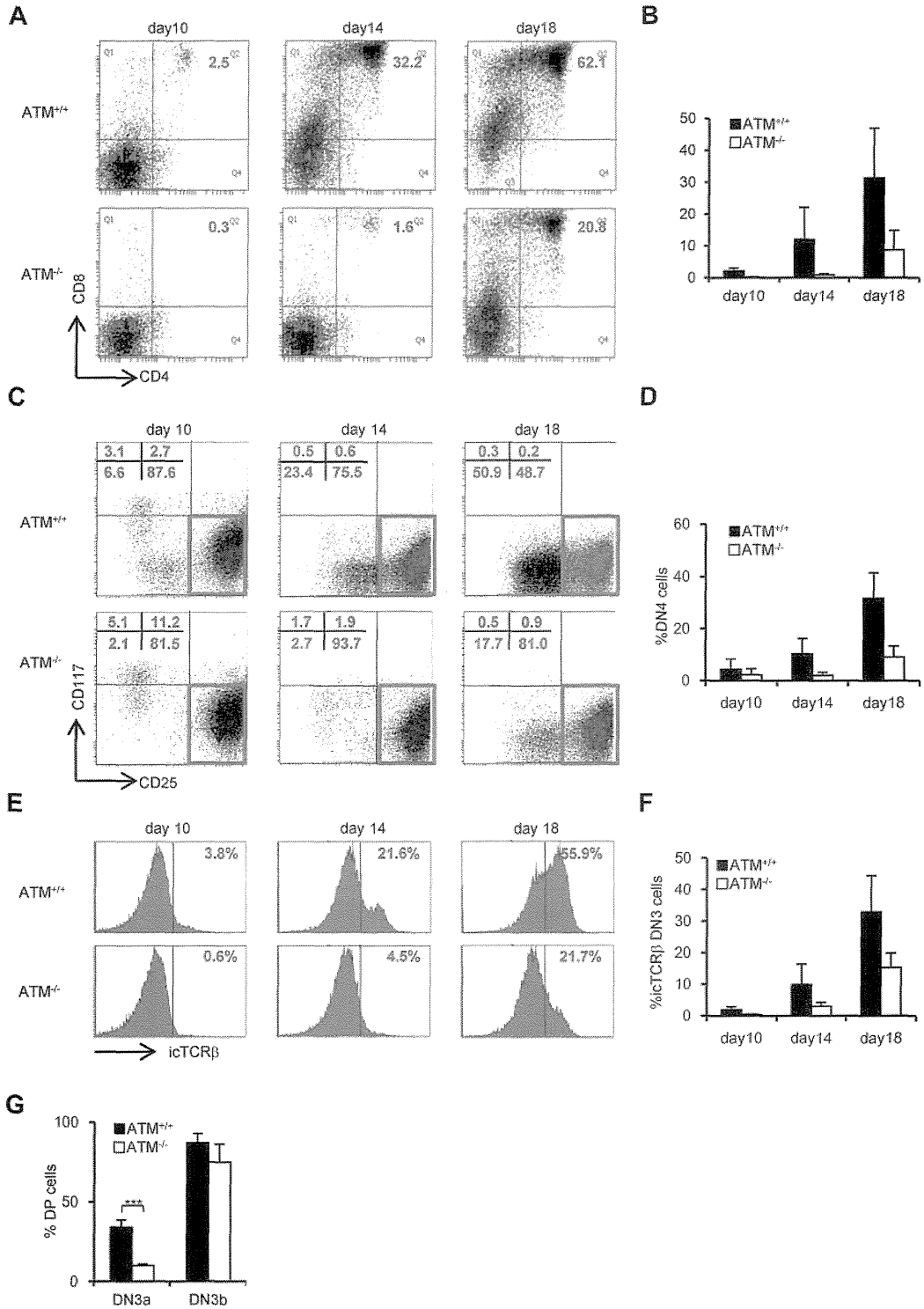

Figure 2. Transition failure from DN3a to DN3b is recapitulated in in vitro culture. Bone marrow progenitors (1×10^4 cells) from 4- to 8-week-old adult BM were cultured with OP9-DLL1 cells supplemented with 5 ng/mL of Flt3L and 1 ng/mL of IL-7 for 18 days. Differentiated cells were harvested on the indicated days. (A) Representative dot plots showing the surface expression of CD4 and CD8 (top) from $ATM^{+/+}$ and $ATM^{-/-}$ BM progenitors. (B) Percentages of $CD4^+CD8^+$ DP phase cells at the indicated time points. (C) Dot plots are gated on DN phase from $ATM^{+/+}$ and $ATM^{-/-}$ BM progenitors. Red squares represent DN3 cells. Representative dot plots are shown when DN3 cells reached 1×10^4 cells. Red dots indicate DN3b cells that are back-gated from the $CD27^+$icTCR-β^+ fraction. (D) Percentages of DN4 phase at the indicated time points. (E) Representative histograms showing expression of icTCR-β on DN3 cells. (F) Percentages of icTCR-β–positive cells on DN3 cells at the indicated time points. Data are representative of 3 independent experiments. Bar graphs represent mean ± SE. (G) Singly sorted DN3a and DN3b cells from each $ATM^{+/+}$ and $ATM^{-/-}$ thymus were cultured on OP9-DLL1. Percentage of cells successfully differentiated to $CD4^+$ and $CD8^+$ (DP) phase were evaluated by flow cytometry on day 4. Bar graph represents mean percentage from 5 independent experiments. Data are mean ± SE. ***$P < .001$.

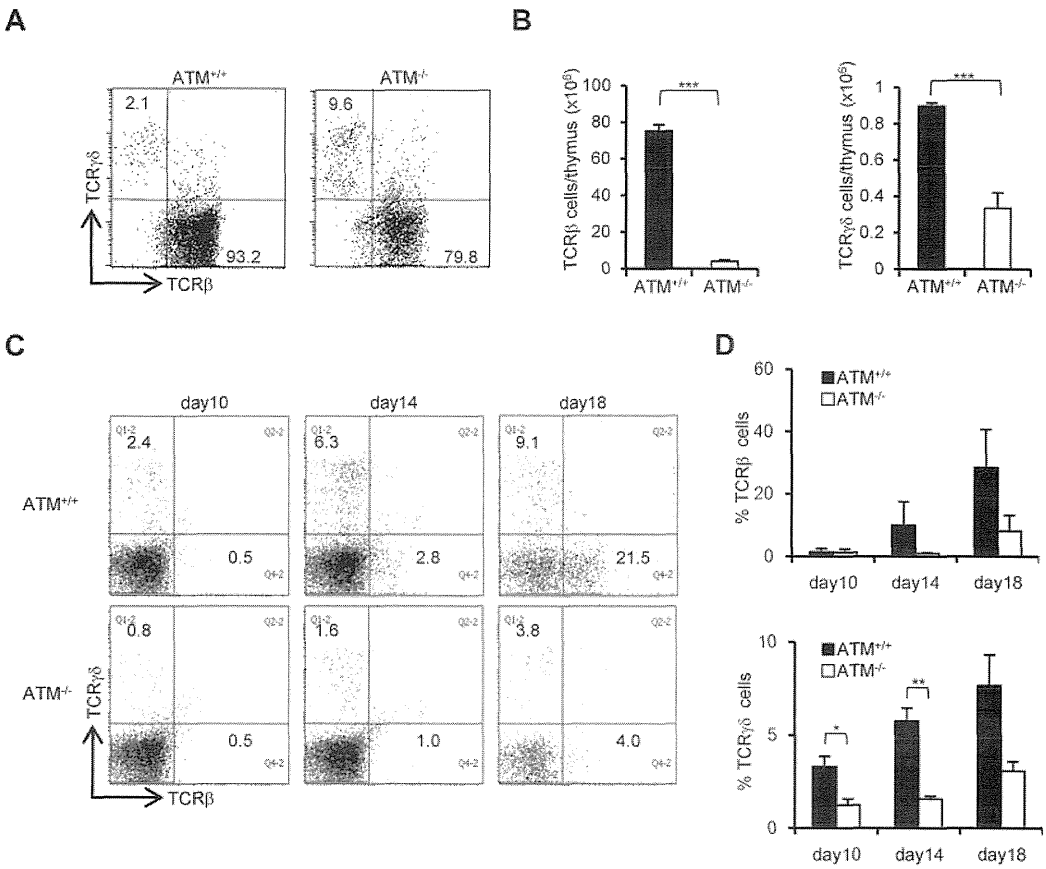

Figure 3. Both αβ and γδ T-cell developments are impaired in the ATM$^{-/-}$ thymus. (A) Dot plots for TCR-β and TCR-γδ expression gated on CD3-positive cells from ATM$^{+/+}$ and ATM$^{-/-}$ thymi. Data are representative of 3 independent experiments. (B) Absolute numbers of TCR-β (left) and TCR-γδ (right)–positive T cells from ATM$^{+/+}$ (n = 4) and ATM$^{-/-}$ (n = 6) thymi. Data are mean ± SE. ***$P < .001$. (C) BM progenitors were cultured with OP9-DLL1 cells supplemented with 5 ng/mL of Flt3L and 1 ng/mL of IL-7 for 18 days. Differentiated cells were harvested on indicated days and stained for surface TCR-β and TCR-γδ. Dot plots are gated on CD45-positive cells from ATM$^{+/+}$ and ATM$^{-/-}$ BM progenitors at the indicated time points. Data are representative of 3 independent experiments. (D) Percentages of TCR-β and TCR-γδ-positive cells at the indicated time points. Data are mean ± SE. *$P < .05$. **$P < .01$.

Nonequivalent TCR-β recombination and an increase in DNA DSBs in ATM$^{-/-}$ thymocytes

It has been shown that ATM$^{+/+}$ and ATM$^{-/-}$ DN thymocytes have nearly equivalent levels of Jδ and Jβ1 signal end joining; however, there are reportedly higher levels of unrepaired Jβ1.1, Jβ1.2, and Jδ1 coding ends in ATM$^{-/-}$ mice.[15] PCR analysis of TCR Dβ1-J1, Dβ2-J2, Vβ1-J1, Vβ4-J1, Vβ8-J1, Vβ1-J2, Vβ4-J2, and Vβ8-J2 recombination in DN2, DN3a, DN3b, and DP stage cells showed almost the same extent of polyclonal rearrangement in ATM$^{+/+}$ and ATM$^{-/-}$ mice (Figure 5A; supplemental Figure 7A-B). However, the Vβ12-J1, Vβ15-J1, Vβ16-J1, Vβ12-J2, Vβ15-J2, and Vβ16-J2 rearrangements were relatively reduced in ATM$^{-/-}$ thymocytes (Figure 5A; supplemental Figure 7B), which is identical to that in thymocytes of mice engineered to express only the RAG2 core protein.[33] Then, we speculated that DSBs at TCR-γ, -δ, and -β loci would remain unresolved in DN3a stage thymocytes of ATM$^{-/-}$ mice. Correspondingly, the frequency of γH2AX-positive cells, a marker for DSBs, was analyzed and shown to be higher in DN2 and DN3 and persist until DP in ATM$^{-/-}$ mice (Figure 5B).

ATM-deficient DN3a cells are defective in cell-cycle regulation and prone to apoptosis

The in vivo cell-cycle profile and level of apoptosis induction were also investigated. Stringent regulation of the timing of gene recombination is crucial for maintaining genomic integrity during normal lymphocyte development. RAG-mediated recombination is limited to the noncycling (G_1) phase of the cell cycle; cells preferentially arrest at G_1 and undergo RAG-mediated TCR-γ, -δ, or -β recombination in the DN3a stage. Cells that successfully achieved normal TCR-γ, -δ, or -β recombination resume cell-cycle progression toward DN3b. Another wave of transient cell-cycle arrest occurs in the early DP phase when the TCR-α locus begins to recombine. Although the cell-cycle profiles of thymocytes in ATM$^{+/+}$ and ATM$^{-/-}$ were not significantly different from one another in the DN2 stage, more ATM$^{-/-}$ cells than ATM$^{+/+}$ cells were observed to be cycling through DN3a into the DP phases (Figure 5C). Furthermore, apoptotic cells were significantly increased in DN3a cells from ATM$^{-/-}$ mice (Figure 5D), corresponding to the previous findings that thymocytes that fail to functionally rearrange the TCR-β chain undergo apoptosis.

Chromosomal breaks at the TCR-α/δ locus and translocations in T-cell progenitors lacking ATM

ATM$^{-/-}$ lymphocytes and leukemia/lymphoma cells exhibit characteristic intralocus rearrangements involving either the TCR or IGH locus.[17,34-36] Chromosomal translocations with gene amplification involving the TCR-α/δ locus were also observed in ATM-deficient mice.[17,37] Based on our findings, we hypothesized that the DN3a to DN3b transition, which is defective in ATM$^{-/-}$ thymocytes, is the window with the highest risk for the formation of

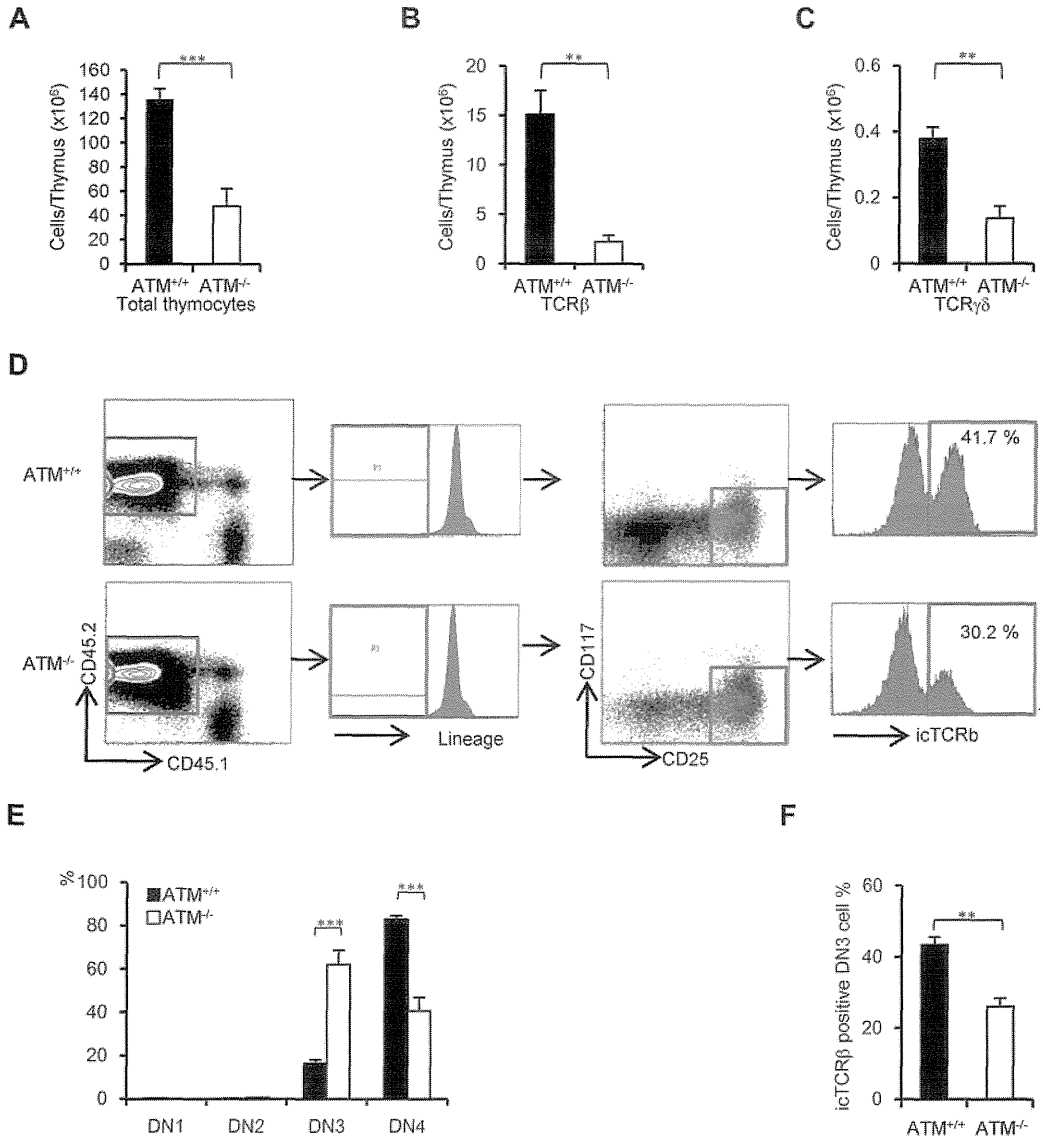

Figure 4. Thymic stromal cells of ATM$^{-/-}$ mice support DN3a to DN3b transition normally. Bone marrow cells from ATM$^{+/+}$ or ATM$^{-/-}$ mice (Ly5.2) were transferred into lethally irradiated ATM$^{+/+}$ mice (Ly5.1). The thymi were harvested from the reconstituted recipient ATM$^{+/+}$ (Ly5.1) mice at 4 weeks after BMT. (A-C) Total thymocytes, TCR-β–positive cells, and TCR-γδ–positive cells were calculated on CD45.2-positive cells. For each group, more than 3 mice were analyzed. (D) Flow cytometric data from ATM$^{+/+}$ thymocytes (Ly5.1) reconstituted with ATM$^{+/+}$ or ATM$^{-/-}$ BM progenitors (Ly5.2). Cells were gated on CD45.2-positive and lineage-negative fractions and analyzed for CD25 and CD117 marker expression. Histograms show icTCR-β positivity in the DN3 phase. DN3b cells as defined by icTCR-β positivity were back-gated to the DN3 fraction and are indicated as red dots. Data are representative of 3 independent experiments. (E) Percentages of DN1, DN2, DN3, and DN4 cells in ATM$^{+/+}$ (Ly5.1) recipient mice that received either ATM$^{+/+}$ or ATM$^{-/-}$ BM progenitors (Ly5.2). Cells were gated on CD45.2 and analyzed. (F) Percentages of icTCR-β–positive DN3b thymocytes in the DN3 fraction in ATM$^{+/+}$ (Ly5.1) recipient mice transplanted and gated as in panel E are shown. Data are mean ± SE. $^{**}P < .01$, $^{***}P < .001$.

chromosome 14 translocations involving TCR-α/δ locus breaks. To monitor chromosome 14 integrity before and after the DN3a phase, an in vitro coculture system, which has been developed by modifying a previously reported system,[38] combined with FISH analysis was performed (supplemental Figure 8). Normal chromosome 14, as shown in red, contains colocalized blue and green foci corresponding to the 5′- and 3′-end of the TCR-α/δ loci, respectively (Figure 6A). Chromosome 14 breaks at the TCR-α/δ locus were observed in 5% of ATM$^{-/-}$ DN2/DN3a cells (54 of 1073 metaphase cells) and 2.5% of ATM$^{-/-}$ DN3b/DN4 cells (11 of 437 metaphase cells; Figure 6B; supplemental Tables 1 and 2), but none in the ATM$^{+/+}$, ATM$^{+/-}$RAG2$^{-/-}$, or ATM$^{-/-}$RAG2$^{-/-}$ cells, indicating that these breaks in ATM$^{-/-}$ thymocytes are RAG-dependent. Chromosome 14 translocations involving the TCR-α/δ locus were occasionally detected in ATM$^{-/-}$ DN2/DN3a cells (1.77%; 19 of 1073 metaphase cells), but not in ATM$^{+/+}$ (961 metaphase cells), ATM$^{+/-}$RAG2$^{-/-}$ (985 metaphase cells), or ATM$^{-/-}$RAG2$^{-/-}$ cells (1034 metaphase cells). Interestingly, the frequency of these chromosomal translocations dramatically increased during the progression to DN3b/DN4 in ATM$^{-/-}$ cell (11.4%; 50 of 437 metaphase cells; Figure 6C; supplemental Tables 1-2). These results suggest that chromosome 14 translocations involving TCR-α/δ locus are mainly generated during DN3a to DN3b transitional stage.

Interestingly, some of the dicentric chromosome 14s carried amplification upstream of the TCRV-α locus (Figure 6D-E), an abnormality that is frequently observed in ATM$^{-/-}$ thymic lymphoma cells (supplemental Figure 9). In this culture system, the

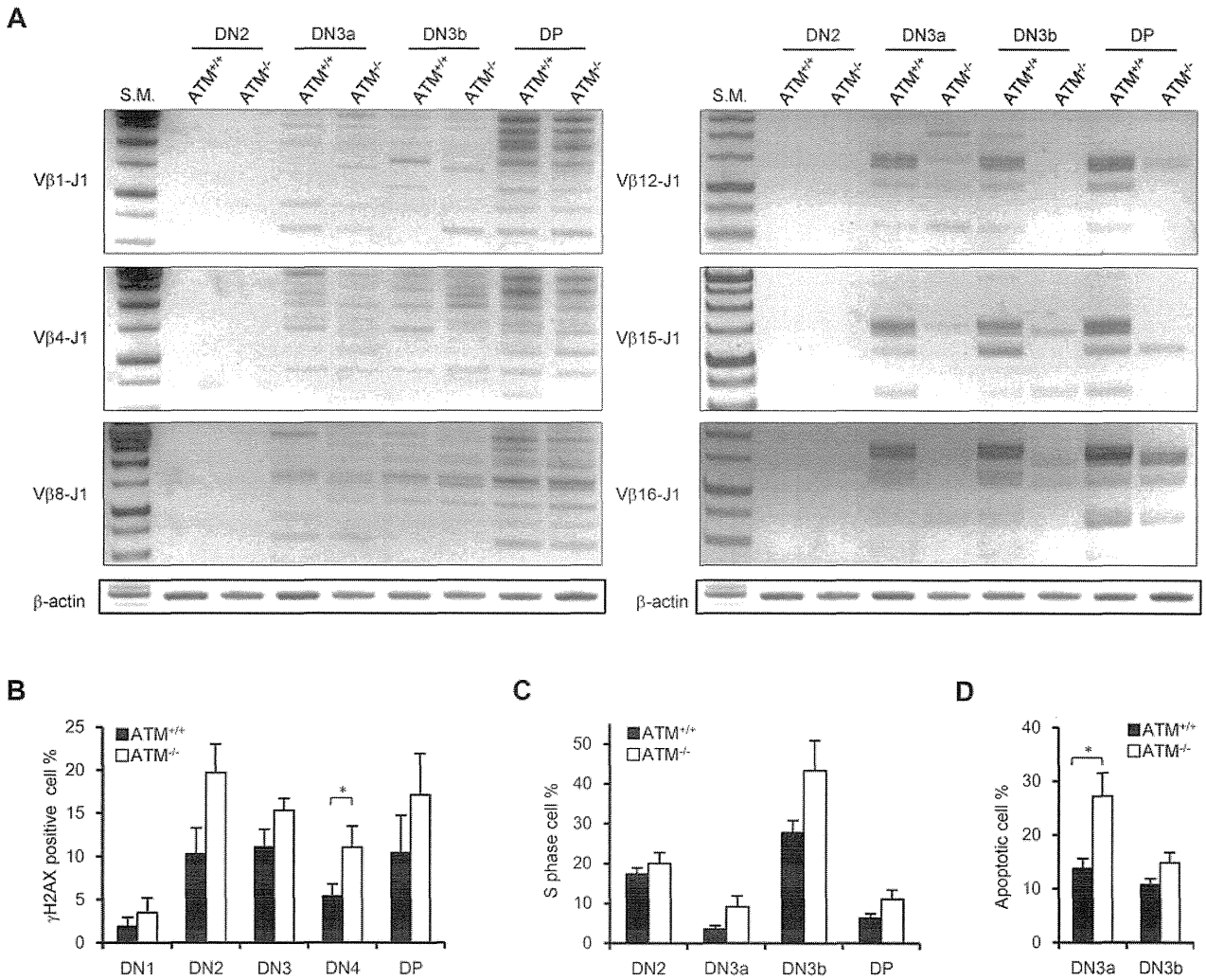

Figure 5. Nonequivalent TCR-β recombination and an increase in DNA DSBs in ATM$^{-/-}$ thymocytes. (A) Rearrangement status of TCR Vβ1-Jβ1, Vβ4-Jβ1, Vβ8-Jβ1,Vβ12-Jβ1, Vβ15-Jβ1, and Vβ16-Jβ1 in the DN2, DN3a, DN3b, and DP stages was analyzed by PCR. (B) γH2AX-positive cell percentages in the DN1 to DP phases by flow cytometry. (C) Percentage of cells in S phase determined by flow cytometric analysis for PI and EdU incorporation at the DN2 to DP stages in ATM$^{+/+}$ (n = 3)and ATM$^{-/-}$ thymocytes (n = 4). (D) Apoptotic cell percentages determined by flow cytometric analysis for annexin V positivity in the DN3a and DN3b stages. Data are mean ± SE. *$P < .05$.

other characteristic abnormalities, including aneuploidy, were also identified during the DN2/DN3a and DN3b/DN4 stages (Figure 6D-E; supplemental Table 3). Sister chromatid breaks in chromosome 12 during mitotic phase and subsequent t(12;14) translocations were also observed in a minor fraction of cells at the DN2/DN3a and DN3b/DN4 stages (Figure 6E; supplemental Figure 10). Chromosome 12, which contains the IGH and BCL11b loci, is often a reciprocal chromosome 14 translocation partner in ATM-deficient thymic lymphoma.

Discussion

In this study, we have visualized, for the first time, the critical developmental step of TCR-α/δ chromosomal breaks and translocations in ATM-deficient thymocytes and narrowed down the DN3a to DN3b stages to be the window for these events.

DN phase differentiation failure in ATM-deficient thymocytes has been speculated to be the result of faulty V(D)J recombination by in vitro studies.[14] Transition failure from DP to SP phase was also reported in in vivo thymus.[8,9] However, accurate profiles for T-cell development at DN phase have not been elucidated in ATM-deficient thymocytes. In addition, some other possibilities need to be ruled out that ATM-deficient thymic stromal cell has negative effect for DN phase development, and ATM itself has roles for a differentiation program, such as transcription factor and signal mediator. We find that DN3a and DN3b differentiation failure is only the result of TCR recombination failure, but not defective thymic stromal cells or aberrant differentiation program in ATM-deficient thymocytes. In the absence of ATM, DN2/DN3a thymocytes were demonstrated to be defective in TCR-γδ and TCR-β recombination, as evidenced by a failure of intracellular TCR-γδ and β expression. They were defective in differentiation toward both αβ and γδ-T-cell lineage in vitro, and absolute numbers of αβ and γδ T cells were decreased in ATM$^{-/-}$ thymus. These findings suggest that T-lymphopenia in ATM-deficient mice is caused by differentiation failure of thymocytes at the early stage from DN3a to DN3b before the stage from DP to SP by defective resolution of TCR breaks.

We demonstrated that the recombinations of TCR Vβ12, Vβ15, and Vβ16-DJ were not successful in ATM$^{-/-}$ thymocytes compared with those of Vβ1, Vβ4, and Vβ8-DJ (Figure 5A). This

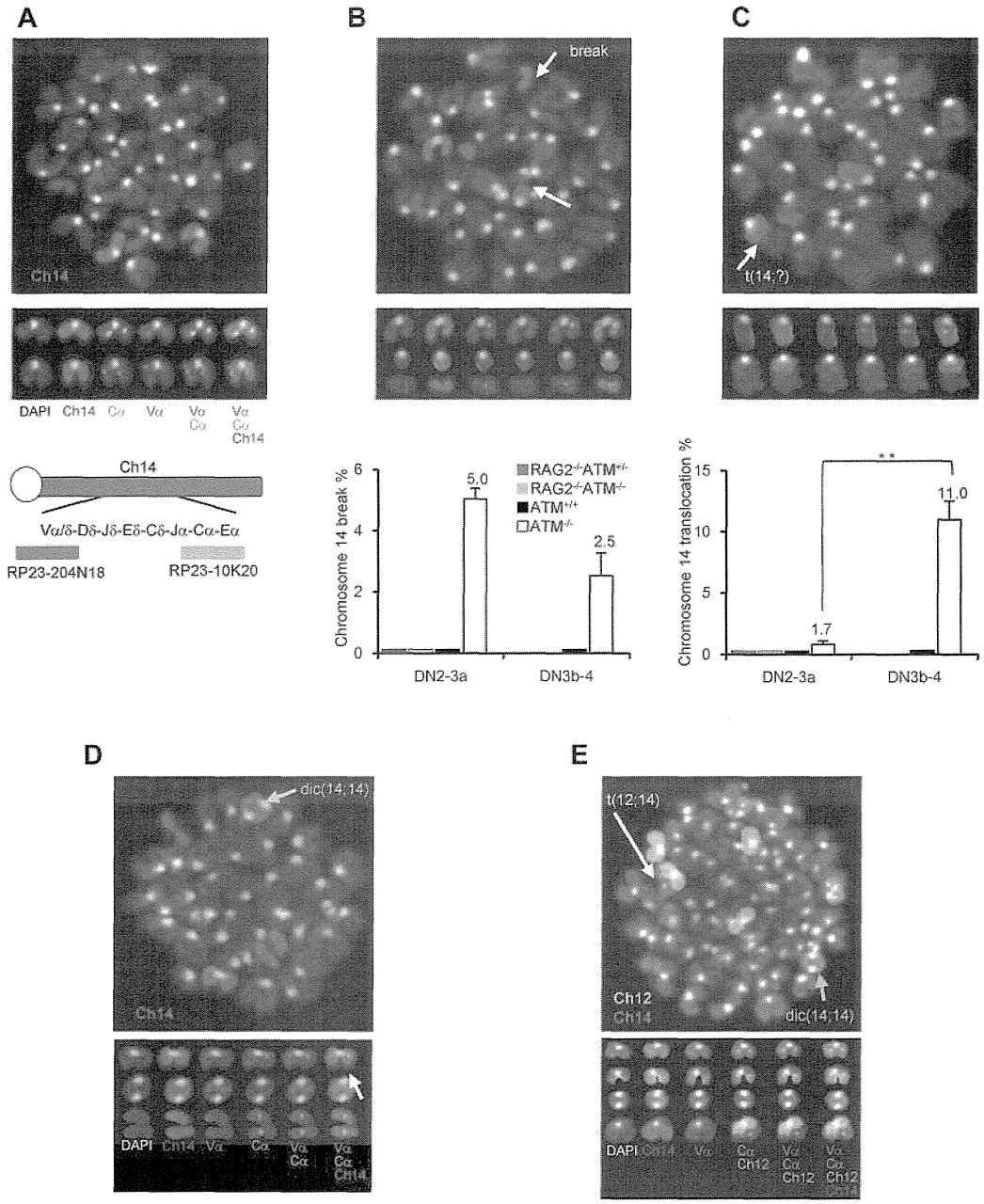

Figure 6. Chromosomal breaks at the TCR-αδ locus and translocations in T-cell progenitors lacking ATM. (A) Normal karyotype; FISH probe hybridized with 5′-TCR-α/δ (blue) and 3′-TCR-α/δ (green). Red represents the chromosomal paint probe for mouse chromosome 14. E indicates defined transcriptional enhancer elements. (B) Representative images of breaks between 5′TCR-α/δ (blue) and 3′TCR-α/δ (green) on chromosome 14 (red; top panel). The percentage of DN2/DN3a cells and DN3b-DN4 cells with a TCR-α/δ locus break is shown in a bar graph (bottom panel). Thymocyte maturation arrests at the DN2/DN3a stage in RAG2$^{-/-}$ mice; thus, DN3b-DN4 phase locus breaks cannot be measured. (C) Representative images of a chromosomal translocations (top panel). The percentage of cells with a chromosome 14 translocations is shown in a bar graph (bottom panel). y-axis indicates change to percentage chromosome 14 breaks and translocations. (D) Representative images of chromosomal abnormalities showing the TCR-α/δ locus on a dicentric chromosome 14 (yellow arrow) and breaks (white arrow). (E) Representative image of a chromosomal 12;14 translocation (white arrow) and a dicentric chromosome 14 (yellow arrow). Data are mean ± SE. $^{**}P < .01$.

skewed pattern of TCR-β recombination is identical to that in thymocytes of mice engineered to express only the RAG2 core protein (Rag2$^{c/c}$; ie, the portion of the molecule that, together with core RAG1, is the minimal region required for in vitro V(D)J recombination). RAG2$^{c/c}$ mice show inefficient recombination for Vβ10, Vβ11, Vβ12, and Vβ15 compared with Vb2 and Vb8 because of a different RSS spacer sequence in these groups.[33] Our findings and these observations seen in the Rag2$^{c/c}$ mouse suggest that ATM and RAG protein might interact or ATM may modify RAG function by phosphorylation or not during recognition of specific RSS sequence for V(D)J recombination. Furthermore, Rag2$^{c/c}$p53$^{-/-}$ mice exhibit similar phenotype with ATM-deficient DN profiles and rapidly develop lymphoma with chromosome translocations at the TCR-δ locus.[37] The defects of T-cell development in these engineered mice are mainly the result of the loss of interaction between the RAG postcleavage complex with ATM and is compatible with our observation in ATM$^{-/-}$ thymocytes.

RAG1 is expressed throughout the cell cycle, whereas RAG2 is periodically destructed at the G_1-to-S transition and is stable only during G_0 or G_1 phase, which limits V(D)J recombination to occur only at G_0 and G_1 cell-cycle phases. Thus, coordinated RAG expression and organized cell-cycle checkpoint are indispensable

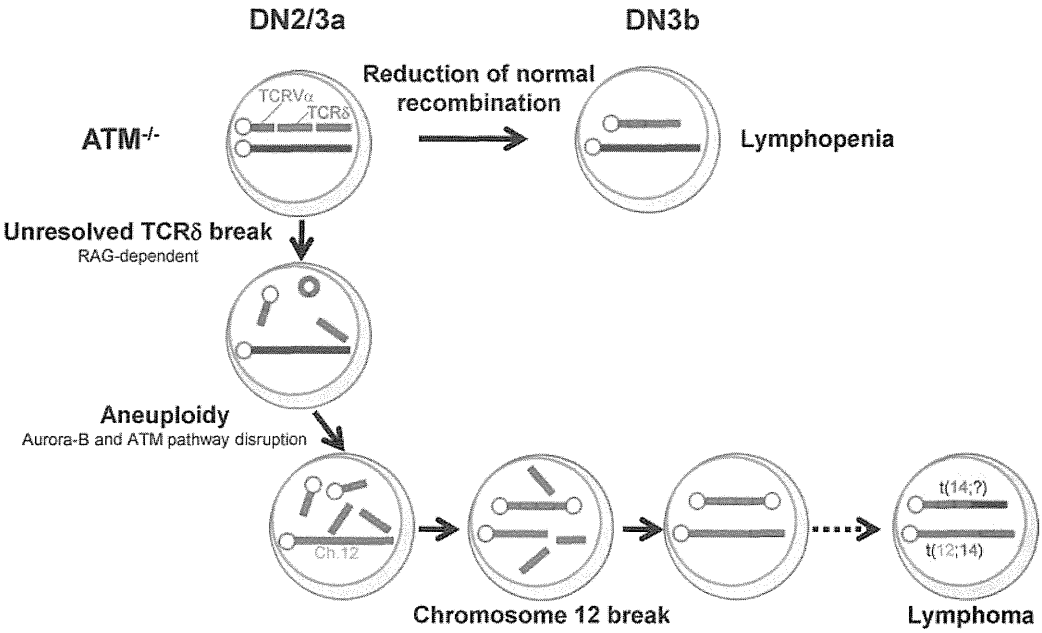

Figure 7. Model for thymocyte development lacking ATM. Schematic illustration for the impaired thymocyte development and creation of a translocation involving the TCR locus.

to prevent aberrant chromosome translocation.[11,39] Cell-cycle deregulation to enter S-phase was observed in phases through DN2 to DP in ATM$^{-/-}$ thymocytes. Thus, it is probable that the G_1-S checkpoint failed to be activated in ATM$^{-/-}$ thymocytes possibly involving or not the failure of Pim2 kinase expression that is mediated by ATM.[40] In our analysis, it was also noted that apoptotic cells were significantly increased in DN3a in ATM$^{-/-}$ thymocytes. Together, these findings unresolved coding end joining concomitant with disorganized cell-cycle checkpoint regulation as well as increased DNA breaks associated with apoptotic nuclear events might lead to genomic instability in early developmental stages of T cells in ATM$^{-/-}$ mice.[41,42]

Our findings led us to propose the following model for the process of generation of chromosome breaks and translocations in ATM deficiency. During DN2/DN3a, RAG-mediated breaks are generated, and they persist beyond the G_1 phase because of defective TCR-β V-DJ recombination and cell-cycle progression. These cells are detected as those carrying chromosomal breaks at TCR-δ on chromosome 14 (Figure 6B). After the DN3b stage, some of these chromosomes recombine with unknown partner chromosomes or occasionally with an inappropriately replicated chromosome 14 itself, leading to dicentric chromosome formation. Occasionally, the upstream TCRV-α locus is amplified by multiple cycles of this process (Figure 6D-E). These findings are reflected by those that aurora-B mediated mitotic ATM activation and the spindle checkpoint play essential roles to suppress aneuploidy.[43] Genomic instability associated with ATM deficiency may also generate chromatid breaks, including chromosome 12, which were observed in minor fraction compared with RAG-dependent chromosome 14 breaks (supplemental Figure 10). Chromosome 12 is a well-known partner of chromosome 14 translocation in ATM$^{-/-}$ thymic lymphoma. The break sites on chromosome 12 are widely spread on 30-Mb-long from IGH locus to centromeric portion involving BCL11b and TCL1 loci, not always involving cryptic RSS,[17] and breaks were detected as chromatid breaks, not as bilateral chromosomal breaks. Taken together, these findings suggest that chromosome 12 breaks presumably occur in RAG-independent manner after completion of sister chromatid synthesis.

These processes, be they random or nonrandom, may lead to chromosome translocations, some of which may somehow get through the checkpoints by successful TCR-γδ or TCR-β recombination and lead to the development of phenotypically normal lymphocytes, yet carrying over oncogenic potentials, after the DN3b/DN4 stages. Loss of genomic guardian systems, such as the ATM-p53 pathway, may enhance additional steps for tumorigenesis.[44] Together with these findings, the initial step of multistep evolutions toward lymphomagenesis was visualized in ATM-deficient thymocytes. RAG-dependent failure during TCR recombination and RAG-independent disruption of chromosomal architecture may be intimately involved in the process for tumor formation.

In conclusion, T-cell developmental failure leading to immunodeficiency and chromosomal translocations involving the TCR-α/δ locus derive from mutually integrated events during the DN2/DN3a stages in ATM-deficient T cells (Figure 7). We propose that our in vitro experimental method is also useful for the functional validation of mutation-targeted therapeutic technologies for AT patients in the future.[45] In light of the finding that 35% of T-cell acute lymphoblastic leukemias carry chromosomal translocations involving *TCR* genes,[46] our findings also suggest that epigenetic dysregulation of ATM or posttranscriptional deregulation of *ATM* gene might be involved in the formation of chromosomal translocations involving *TCR* genes in some T-cell leukemias with an apparently normal *ATM* gene.

Acknowledgments

The authors thank P. J. McKinnon for providing ATM$^{+/-}$ mice; M. F. Greaves, P. D. Burrows, and K. Enomoto for critical reading for manuscript; and Y. Kutami for technical support.

This work was supported by a Grant-in-Aid from the Ministry of Education, Science, and Culture (Japan) and Grant-in-Aid from the Ministry of Health, Labor and Welfare (Japan; M.T. and S.M.).